NUMERICAL INVESTIGATION OF THERMAL MANAGEMENT FOR AN AIRFOIL PROFILE TO PREVENT ICE FORMATION

A Thesis submitted to
the Graduate School of Engineering and Science of
İzmir Institute of Technology
in Partial Fulfillment of the Requirements for the Degree of

MASTER OF SCIENCE

in Mechanical Engineering

by
Çağatay KÖK

July 2019
İZMİR

We approve the thesis of **Çağatay KÖK**

Examining Committee Members:

Assoc. Prof. Dr. Erdal ÇETKİN
Department of Mechanical Engineering, İzmir Institute of Technology

Prof. Dr. Tahsin BAŞARAN
Department of Architecture, İzmir Institute of Technology

Prof. Dr. Aytunç EREK
Department of Mechanical Engineering, Dokuz Eylül University

16 July 2019

Assoc. Prof. Dr. Erdal ÇETKİN
Supervisor, Department of Mechanical Engineering, İzmir Institute of Technology

Prof. Dr. Sedat AKKURT
Head of the Department of Mechanical Engineering

Prof. Dr. Aysun SOFUOĞLU
Dean of the Graduate School of Engineering and Science

ACKNOWLEDGMENTS

First of all, I would like to thank my esteemed supervisor, Erdal ÇETKİN, for his endless patience, help and guidance throughout the study. Without his understanding and support, I would not have been able to complete this study. I would also like to thank Prof. Dr. Tahsin BAŞARAN and Prof. Dr. Aytunç EREK for sparing from their valuable time.

I would also like to thank my dear and respected colleagues at Bosch Termoteknik for their support during my thesis process. I will always be grateful for their understanding and help.

Last but not least, I would like to thank my precious family, who have supported me for all my life, in every step I took.

ABSTRACT

NUMERICAL INVESTIGATION OF THERMAL MANAGEMENT FOR AN AIRFOIL PROFILE TO PREVENT ICE FORMATION

In this study, we present a design alternative to prevent the icing of a wind turbine blade in the cold climate wind zones. The main objective is to create a thin film around the wing profile that can protect the surface from ice formation. In order to form this insulating layer, the leading edge, which is the region where the icing started first, the circular openings that could provide hot air to the outside of the wing, were added to geometries. By means of these openings, it has been tried to provide a solution that will prevent ice on the surface without the need to heat the entire wing. At the same time, the effect of these openings on the wing, the distance between the openings and the positions and diameters of the wings on the lifting performance of the wing were investigated. Throughout the study, the design parameters were all proportional to the chord length of the wing. In the model stage, instead of the entire wing, only one section of the wing was modeled using symmetry boundary conditions in order to use the existing limited computing power more efficiently. In this way, both the number of network elements and the calculation time can be modeled in such a way that the distance between the openings is equal to the width of the section. The results show that the lifting force, as can be expected, is small. As the width, i.e. the distance between the openings increased, the lifting force became more stable, while the film layer temperature decreased.

Keywords and Phrases: Wind turbine, Cold climate, Thermal management, Anti-ice, De-ice; Ice accretion

ÖZET

BİR KANAT PROFİLİ İÇİN BUZ OLUŞUMUNUN ENGELLENMESİNDE ISIL YÖNETİMİN NUMERİK OLARAK İNCELENMESİ

Bu çalışmada, bir rüzgar türbini kanadının, soğuk iklim rüzgar sahalarında buzlanmasını engelleyecek bir dizayn alternatifi sunulmuştur. Temel amaç, kanat profilinin etrafında, yüzeyi buz oluşumundan koruyabilecek ince bir film tabakası oluşturmaktır. Bu izolasyon tabakasını oluşturabilmek için buzlanmanın ilk olarak başladığı bölge olan uç bölgesine, kanadın dışına sıcak hava verebilecek dairesel açıklıklar eklenmiştir. Bu açıklıklar vasıtasıyla, kanadın tamamını ısıtmaya gerek kalmadan, sadece yüzey üzerinde buzlanmayı engelleyecek bir çözüm üretilmeye çalışılmıştır. Aynı zamanda bu açıklıkların kanat boyunca aralarındaki mesafenin, kanat üzerindeki konumlarının ve çaplarının, kanadın kaldırma performansına olan etkisi incelenmiştir. Çalışma boyunca tasarım parametrelerinin hepsi kanadın kord uzunluğuna oranlanmıştır. Model aşamasında, mevcut limitli hesaplama gücünü daha verimli kullanabilmek adına, tüm kanat yerine, kanadın sadece bir kesiti simetri sınır koşulları kullanılarak modellenmiştir. Böylelikle hem ağ elemanı sayısından ve hesaplama süresinden kara geçilirken, hem de açıklıklar arası mesafe kesit genişliğine eşit olacak şekilde modellenebilmiştir. Sonuçlara bakıldığında, kaldırma kuvvetinde, tahmin edilebileceği gibi, ufak kayıplar görülmüştür. Genişlik, yani açıklıklar arası mesafe arttıkça kaldırma kuvveti daha stabil bir hale gelirken, film tabakası sıcaklığında düşüşler gözlemlenmiştir.

Anahtar Kelimeler ve İfadeler: Rüzgar türbini, Soğuk iklim, Termal yönetim, Anti-buz, Buz oluşumu, Buzlanma

TABLE OF CONTENTS

LIST OF FIGURES

Figure **Page**

LIST OF TABLES

LIST OF SYMBOLS

p	Pressure on airfoil surface	N/m^2
N	Normal force	N
A	Axial force	N
L	Lift force	N
D	Drag force	N
c	Chord length	mm
V	Velocity	m/s
ρ	Density	kg/m^3
C	Dimensionless coefficient (wing)	
c	Dimensionless coefficient (airfoil)	
P	Pressure	Pa
M	Momentum	N/m
d	Pressure inlet diameter	mm
w	Section width	mm

Greek Letters

α	Angle of attack (AoA)	degree
β	Angle of pressure inlet	degree
τ	Shear stress	N/m^2

Subscripts

L	Lift(wing)
l	Lift(airfoil)
D	Drag(wing)
d	Drag(airfoil)
dyn	Dynamic
∞	Freestream

Superscripts

‘	Per unit length

CHAPTER 1

INTRODUCTION

1.1. Wind Turbines

A wind turbine can be described as an energy converter device. It takes the kinetic energy of wind and converts it to mechanical energy, then the electricity. Modern wind turbines mostly considered as descendants of windmills[1].

Even though it is possible to see many different designs, wind turbines can be categorized into two main sections:

- VAWT (Vertical Axis Wind Turbine)
- HAWT (Horizontal Axis Wind Turbine)

In this study, an airfoil from a HAWT design is chosen. Examples are represented in the following figures.

Figure 1. A group of HAWTs (Source:[2])

Figure 2. A group of VAWTs (Source:[3])

At this point, for the future references in this study, it is the most beneficial to mention the main parts of the wind turbines.

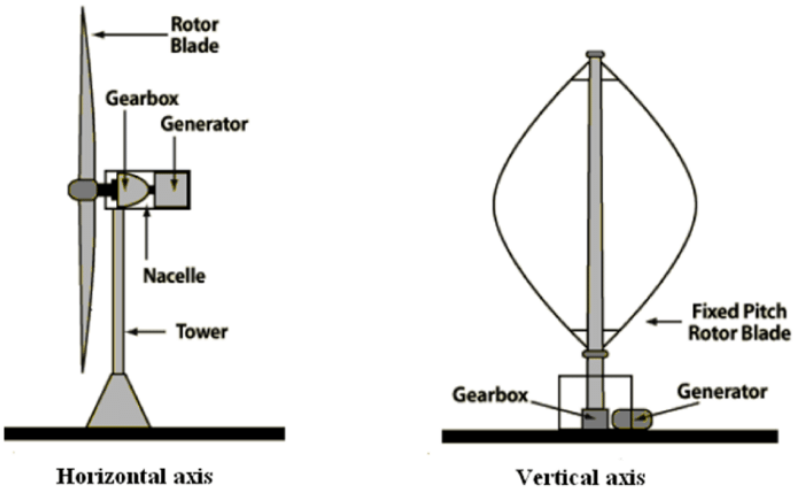

Figure 3. Main sections of the wind turbines (Source:[4])

As it is given in Figure 3, a HAWT basically consists of three primary parts; rotor blades, nacelle, and tower. While nacelle encapsulates gearbox and generator, rotor blades are the main driver of the system. As they face the wind, thanks to their aerodynamic designs, they can harvest wind energy and convert it to shaft work. This shaft work is directly delivered to the nacelle, then transformed to electricity.

1.2. Cold Climate Sites

It is possible to classify wind farm sites regarding their technical characteristic features. An open site without any obstacle to disturb wind turbines with extensive meteorological data, which is close enough to electrical lines with acceptable space to any populated region can be addressed as a conventional site. On the contrary, a nonconventional site has wind turbines face with extreme environmental conditions. These conditions can be directly linked to topological aspects of the site or the meteorological conditions. A cold climate site can exhibit a number of features from both categories. Basically, the regions where the air temperature is below zero for long periods during the year, where terrains are complex, about 700~800 meters above sea level, can

be defined as the cold climate sites[4]. It is possible to see water content in the air, and extreme conditions like high turbulence, hail, lightning are likely possible.

Wind turbines in cold climates regularly face with icing conditions. Ice formations on blades or nacelle can crucially affect considerations of efficiency, maintenance and safety issues. Despite this fact, regions likely to have icing conditions still can be a candidate for wind turbine installations. In cold climate regions, for the first 1000m wind speed increases 0.1 m/s per each 100m altitude[5]. Also, a site with such features might be the only option for a wind farm (i.e. sub-Arctic regions, China, Russia, Finland, Canada, cold desert regions)[4].

Despite the advantages mentioned above, it is possible to witness harsh penalties in terms of efficiency when we talk about a wind turbine operating in icing conditions.

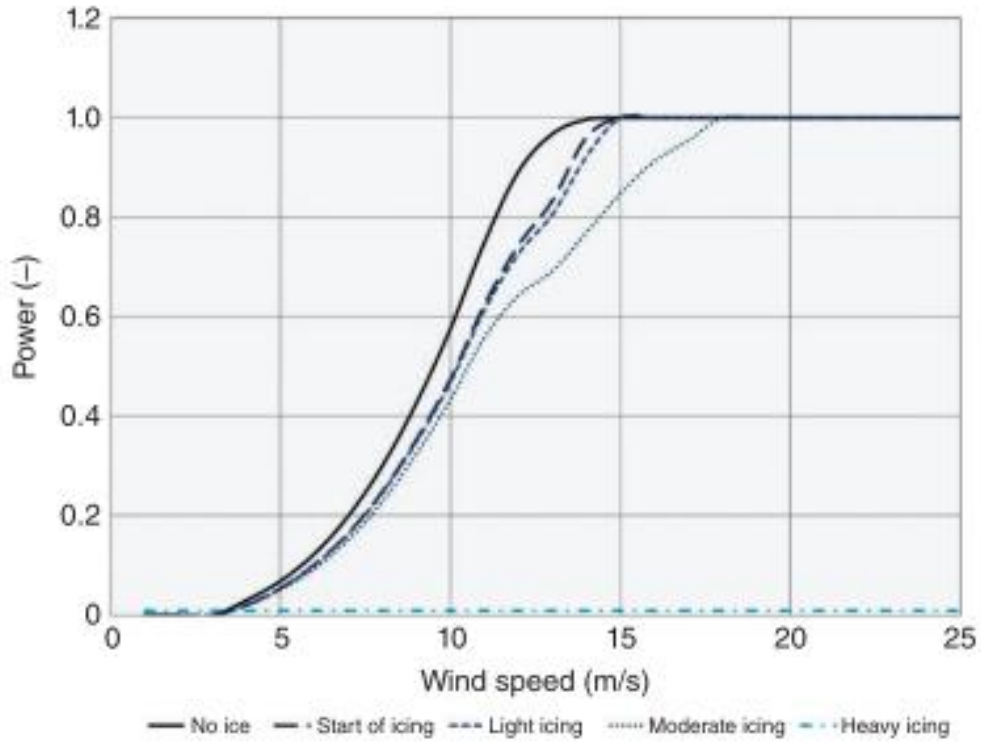

Figure 4. Effect of icing on performance(Source:[6])

The effects of icing on the performance of a wind turbine is well represented in Figure 4. Also, potential annual energy production loses in a cold climate site in Québec, Canada provided by the International Energy Agency is given in Figure 5.

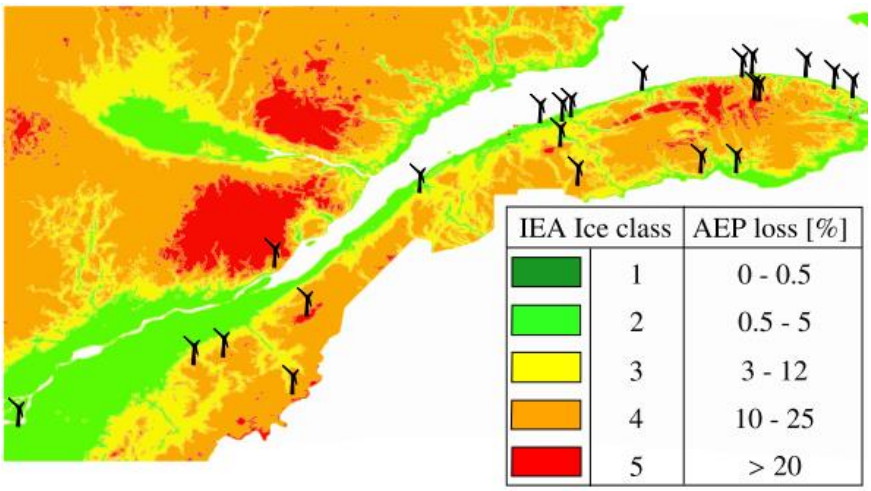

Figure 5. Cold climate farming layout and AEP loss(Source:[7])

The icing on wind turbine blades might cause several problems including decreased performance in aerodynamics, change in natural frequency of the turbine, and extra loads on the blades. Aside from the blade aspect of the problem, functionalities of measurement instruments are disquieting matter. Any continuous false read from sensors directly affects control of wind turbine, thus efficiency. Main problems due to ice formations on blades can be listed as follows[8] :

- The full stop of the operation
- Change in aerodynamic character
- Overloading on blades
- The decrease in fatigue life
- Safety problems / Thrown ice

There are lots of different aspects to consider for a cold climate wind turbine project. Laakso[9] gives keynotes about the challenging conditions of the region to be chosen and the points to be taken into consideration in his work rather than the formation of ice. When a complete cold climate project is considered, it is necessary to touch on many points, from work safety to location accessibility, from accurate measurements to project construction.

1.3.Icing Prediction

Earlier works are mostly regarding aircraft icing problems. In order to address problems and models adequately, icing formations can be categorized depending on the fouling mechanism. A “rime” icing can occur air temperatures below -10^{o}C and results in increased drag, decreased lift, and more weight on the wing even though it is uniformly distributed along the surface. A “glaze” icing, however, occurs between temperatures 0^{o}C to -10^{o}C when wing meets a wind with water contamination (cloud). This time icing is triggered by the released latent heat from the impact between droplets and wing surface. Starting from the leading edge, water droplets find their way to colder areas on the wing. Consequences of fluctuations of lift and drag might be stern[10].

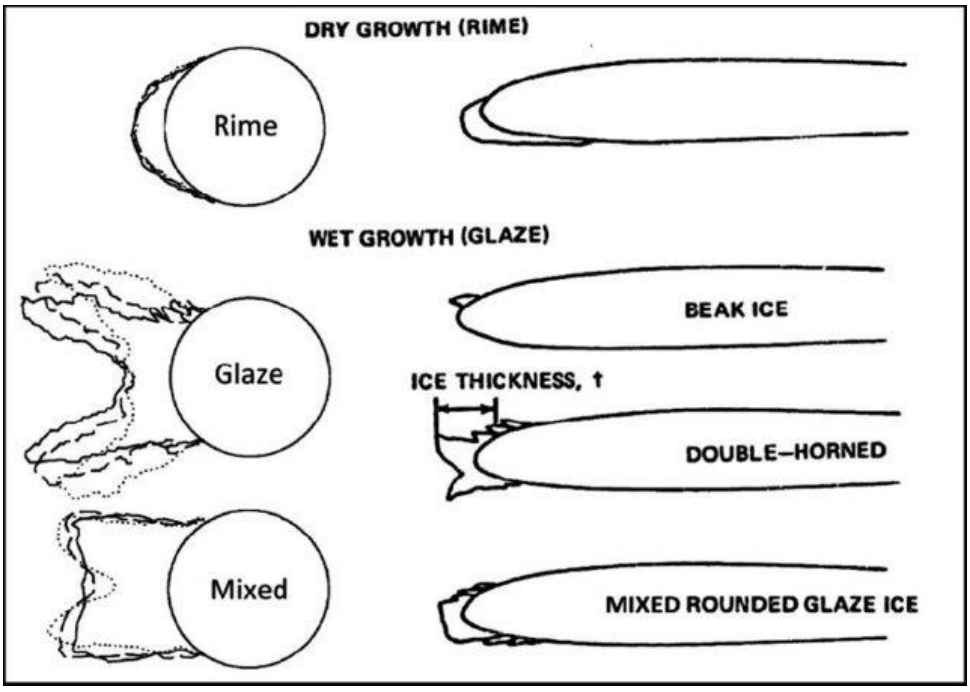

Figure 6. Icing types and locations(Source:[10])

In order to be able to foresee the consequences of ice accretions on the aerodynamic performance of airfoils, numeric models for icing prediction are extensively studied.

MacArthur et al. published the progress of LEWICE, a time-dependent model for ice accretion. LEWICE has been developed by University of Dayton Research Institute (UDRI), and it is a supplementary work to prior studies[10]. They present a general

schematic of the algorithm of their codes and also a comparison of results with experimental studies. Another study of MacArthur is a numerical simulation of accretion using LEWICE on NACA 0012 airfoil[11]. In this study, he compared results from the model to experiments carried out by NASA.

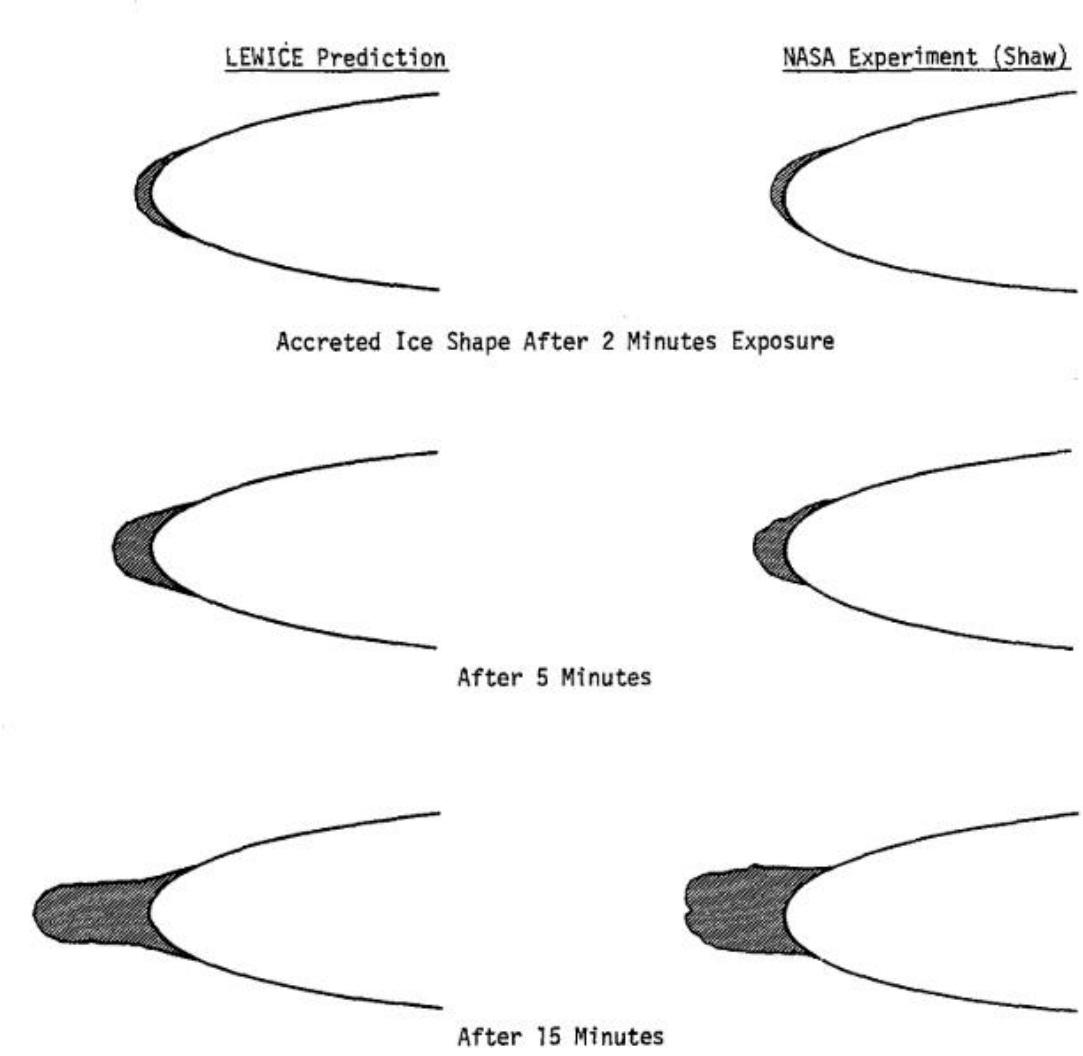

Figure 7. Predicted and observed ice accretion shapes under rime conditions for a NACA 0012 section at 0^{o} angle of attack, Conditions: The figure shows roughly the first 20% of the chord (Source:[11])

In the same manner, Guffond et al. published a technical report about the validation of 2D ice accretion code ONERA[12]. Another code called TRAJICE2 was introduced by Gent[13]. It was a water droplet trajectory and ice accretion prediction program. In 1997, Wright, Gent, and Guffond published a collaborative review about LEWICE/ONERA/TRAJICE2 codes[14].

In their study, Fortin et al.[15] examined the relationship between the icing effect on wind turbines and meteorological parameters, as well as the best position of a de/anti-icing system on an airfoil profile. While determining the best location for a system, they predicted the trajectory of fluid flow with water particles in it, and then studied ice accumulation numerically.

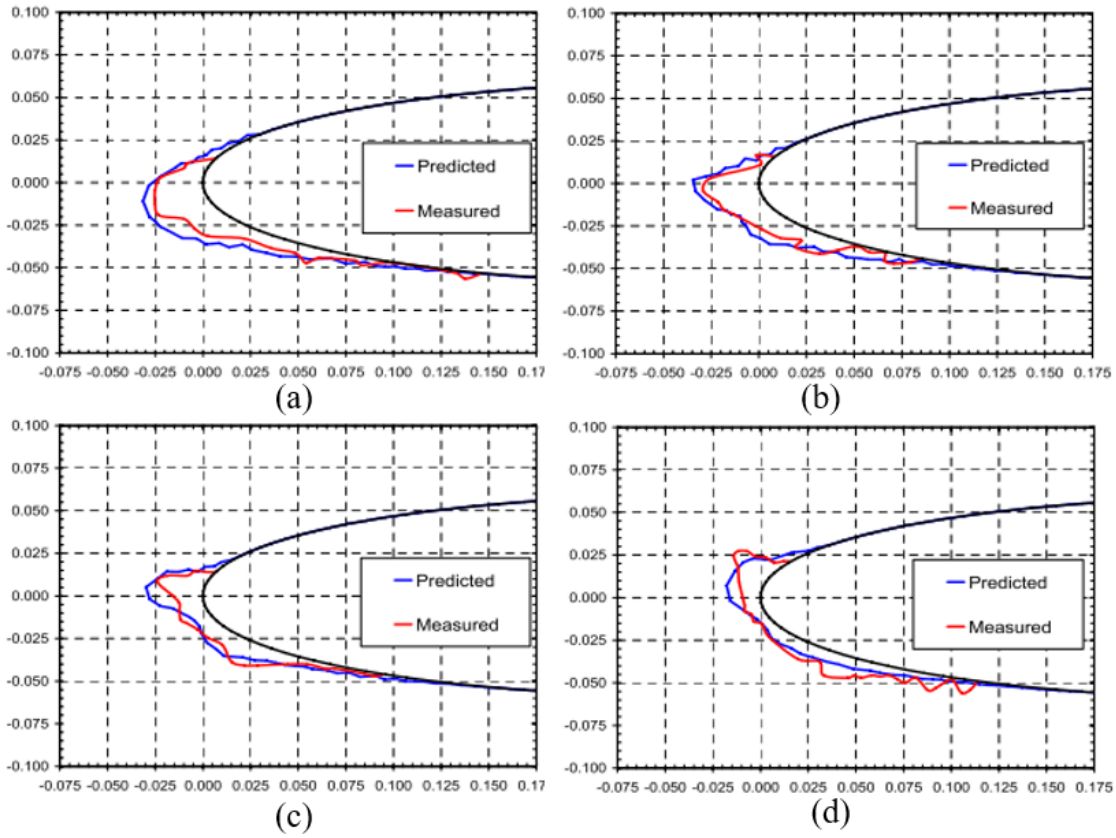

Figure 8. Ice shapes at different temperature. (a) At -28.3ºC (b) At -13.3ºC (c) At -7.8ºC (d) At -4.4ºC (Source:[15])

Hu et al.[16] numerically investigated rime occurrence on the NREL Phase VI blade. First, they generated an icing model. The validation of their study is satisfactory, as the error for the ice shape area is 1,5% and 2,4% for the rotating blade. They concluded ice thickness can reach up to 7,7cm, and also it can accumulate 105,3% mass wise along the radial direction of the rotor.

1.4.De/Anti-Icing Solutions

Even though none of them has become a standard, solutions for icing problem can be found in the literature. Since fundamentals are the same, it is seemly to consider applications on aircraft wings as well. Mentioned solutions can be classified as active and passive methods. Whereas active methods require energy supplied to work, passive ones do not require such supply[8].

Where anti-icing is the prevention of any ice accretion, de-icing systems are here to get rid of already developed ice formations. Earlier methods include thermal melting, surface deformations, and freezing point depressants. In the thermal melting method, heat flux is applied to the cold surface to melt any ice formations. However, as a drawback, water might run along the surface, which results in runback ice. Surface deformation methods relatively require less energy. This method has structures that can deform the profile abruptly in the region at the front of the wing profile. Thus, when they are activated, they break the formed ice by cracking. Another solution is to alter the phase change mechanism by additives. For example, spraying a liquid which increases the freezing point to the surface of the wing can be a useful solution[17].

Figure 9. Working principle of surface deformation method (Source:[18])

As the icing on the leading edge of a blade tends to follow the airfoil profile, any amount of ice introduced to the blade can result in different characteristic behavior of the blade. This change can be explained by the fact that the icing creates its own lifting and friction forces. With the effect of these forces on the system, the wing starts to work in a different scenario than the one designed. The newly introduced ice formation in the system changes the loading on the wing as well as the efficiency and the aerodynamic characteristics. The forces formed, alters the lifetime of the turbine as well as the operation[18].

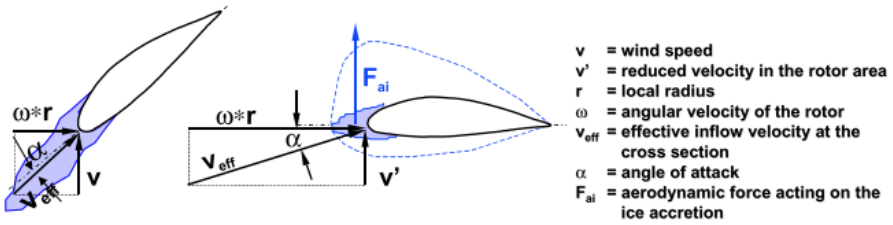

Figure 10. Extra loading scenario due to ice accretion (Source:[18])

Few of the solutions are more frequently discussed in recent years. Placing electrical resistance heaters to the leading edge of wings is one of them. This solution applied in the mid-90s to wind turbine technologies[19]. It is possible to see patent applications in literature for both aircraft[20] and wind turbine[21] wings.

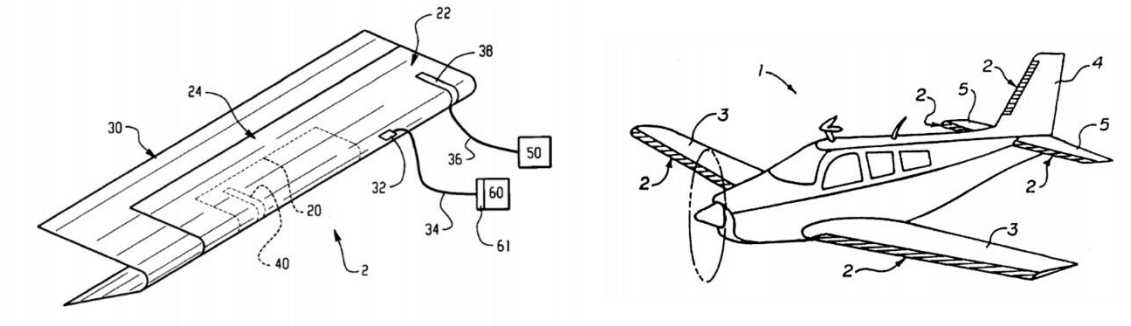

Figure 11. Heating pads idea for aircraft (Source:[20])

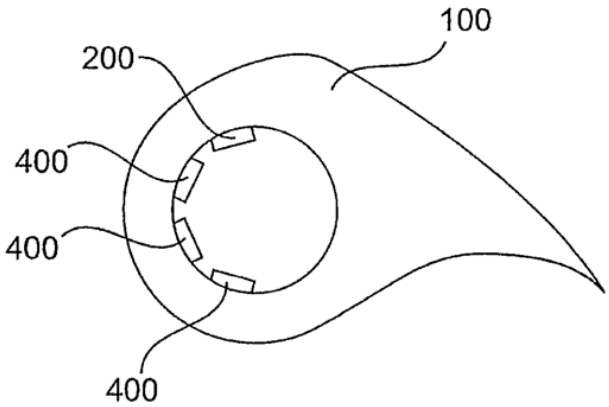

Figure 12. Cross-section image of heating pads of wind turbine application patent(Source:[21])

A related mathematical model of thermal boundary layers on a nonisothermal airfoil surface with evaporation is studied by Silva et al.[22]. They proposed a mathematical model for an electrothermal anti-ice system. They carried out calculations

in order to determine the operational parameters of an electrothermal anti-ice system. As they stated, the heat transfer layer between the surface of the profile and the fluid is sensitive to the surface temperature and evaporation, the solution of the thermal boundary layer needs attention. The most striking part of their models is that, rather than abruptly, they have calculated transition from laminar to turbulence continuously and smoothly. There are some problems introduced by this possible solution as well:

- Heating elements may attract lightning
- Failure of one element may cause the imbalanced mass distribution of ice
- Laminated heating elements may increase surface roughness
- Electrical consumption of heaters may exceed turbines maximum output power

Heating inside volume of wings by convection applied on an Enercon turbine in Switzerland[8]. An extensive study has been carried out by Rodriguez[23] for aircraft wings. He modelled a solution, in which the inner surface of the leading edge is heated by hot air. One downside of this solution is directly related to blade material. Composite materials used in wind turbine blade manufacturing have a high thermal resistance. As span length of a wing increases, layers of composite material increase as well. As shell structure increases in thickness and length, in order to keep the outer surface at a certain temperature, supplied air temperature needs to be higher.

In 1996 Yukon Energy applied a black, non-wetting, impact resistant coating called StaClean[24]. It is an example of passive methods. However, the black colour of the coating did not work as presumed. Some parts of blades with original colour reached higher temperatures[8].

Study of Karmouch et.al.[25] is another example of coatings, a passive system to prevent the freezing of cold climate wind turbines. The main objective in their work is to use the ice-phobic coating PTFE (polytetrafluoroethylene) to separate the ice from the profile surface by the help of wind and/or gravity. At the end of the study, where the application conditions of the coating were given, it was seen that the PTFE coating resulted in a reduction of 80% in the adhesion compared to the original surface.

Inserting a heating element to de-ice is one of the common practices. Investigation of the behaviour of such a solution is also important. In their study, Yaslik et al. [26] generated a calculator that solves the deicing problem in a 3D unit of multi-layered composite element.

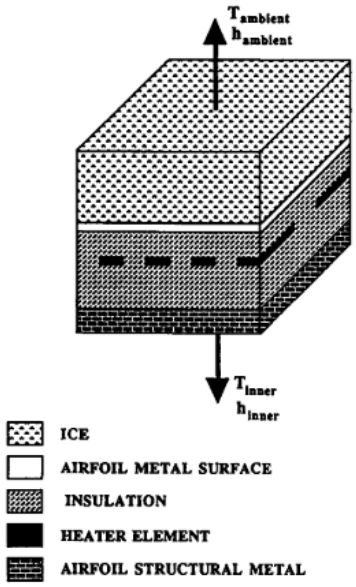

Figure 13. Material layer defined in the 3D model[26]

Their numerical model included assumptions of perfect ice(uniform thickness without any air pockets), perfect thermal contacts, constant material properties, and phase-change over a small range of temperature instead of a single melting point. Their code showed good agreement when compared to the experimental results.

1.5.Incompressible Flow Over Airfoils

In order to accurately describe the framework of the study, it is important to examine the incompressible flow around the airfoils. Mainly there are two basic sources of aerodynamic forces and moments no matter how complex geometries seem; pressure distribution and shear stress distribution over the aerodynamically interested body surface[27].

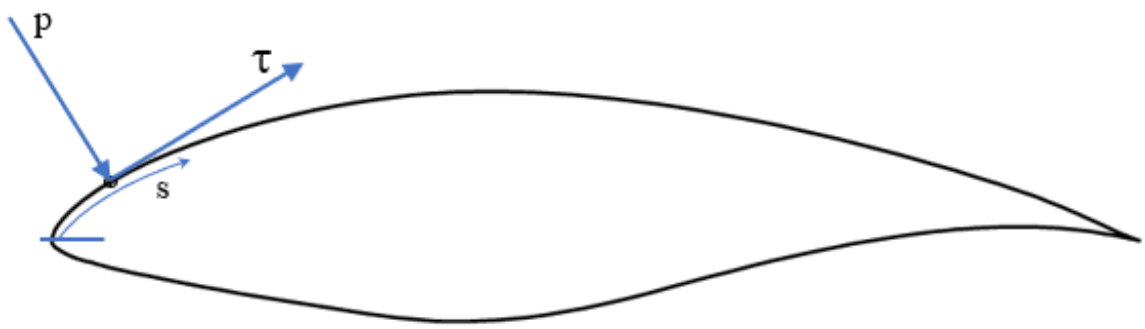

Figure 14. Stress distributions on an airfoil

While p acts normal to the surface, τ is tangential. Both of them are functions of the position on the surface.

$$p = p(s) \text{ = distribution of surface pressure} \quad (1.1)$$
$$\tau = \tau(s) \text{ = distribution of shear stress} \quad (1.2)$$

Integrating Eq.(1.1) and Eq. (1.2) along the surface s, gives the resultant force R and moment M on the body.

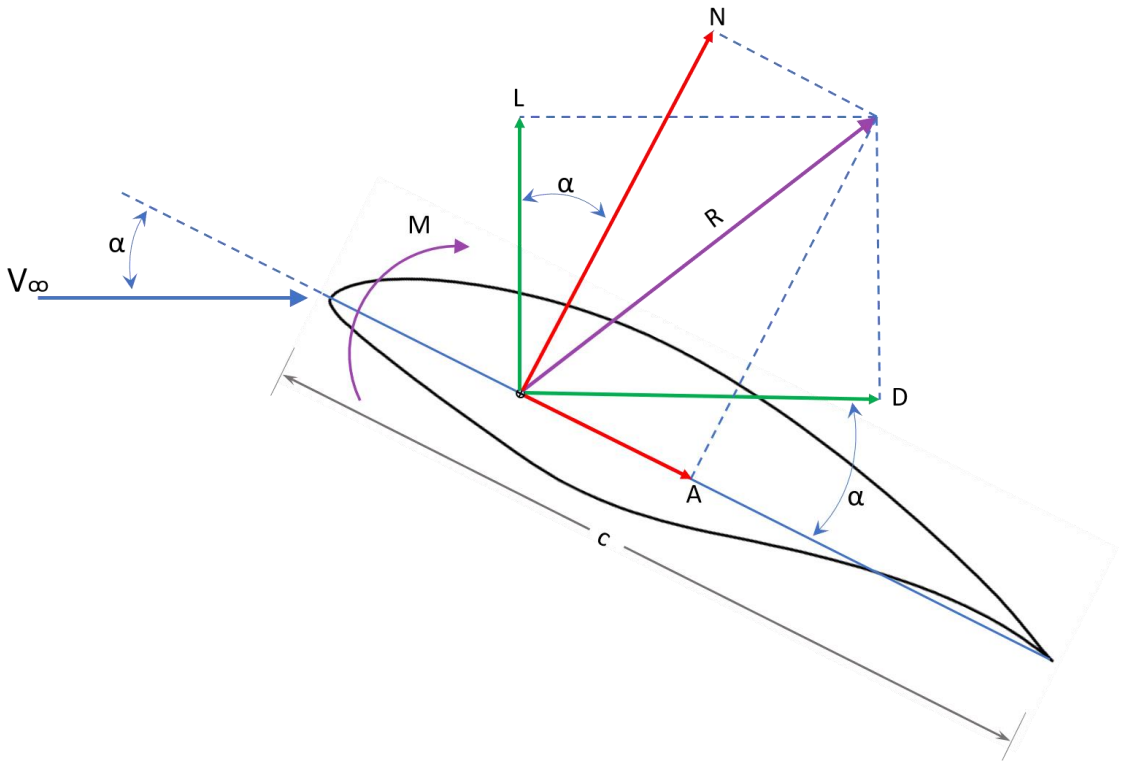

Figure 15. Aerodynamic forces acting on an airfoil

Resultant force R can be divided into its components. There are two couple of forces that directly represent R. Lift force L is the component R perpendicular to the freestream velocity V_∞, whereas drag force D is parallel to the V_∞. Normal force N however, is perpendicular to chord c, while axial force A is parallel to chord c. The angle of attack α is described as the angle between freestream velocity and chord. Therefore, it is possible to express geometrical relation between the force couples.

$$L = N\cos\alpha - A\sin\alpha \quad (1.3)$$
$$D = N\sin\alpha + A\cos\alpha \quad (1.4)$$

Since the descriptions of forces are given, execution of integrals of pressure and shear stress distributions can be detailed.

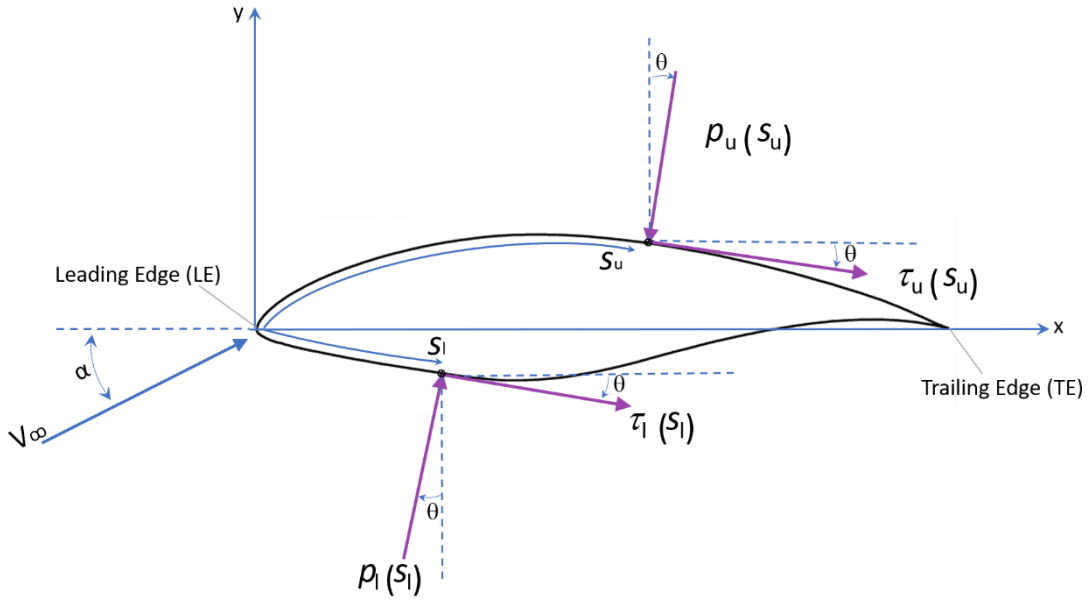

Figure 16. Stress components along an airfoil

As mentioned before, p and τ are a function of position. For the ease of calculation, the upper and lower sides of the airfoil can be addressed separately.

For the upper body surface:

$$dN'_u = -p_u ds_u \cos\theta - \tau_u ds_u \sin\theta \quad (1.5)$$
$$dA'_u = -p_u ds_u \sin\theta + \tau_u ds_u \cos\theta \quad (1.6)$$

For the lower body surface:

$$dN'_l = p_l ds_l \cos\theta - \tau_l ds_l \sin\theta \quad (1.7)$$
$$dA'_l = p_l ds_l \sin\theta + \tau_l ds_l \cos\theta \quad (1.8)$$

In order to obtain total normal and axial forces per unit span, equations (1.5) to (1.8) should be integrated along the chord starting from the leading edge:

$$N' = -\int_{LE}^{TE} (p_u \cos\theta + \tau_u \sin\theta) ds_u + \int_{LE}^{TE} (p_l \cos\theta - \tau_l \sin\theta) ds_l \quad (1.9)$$

$$A' = \int_{LE}^{TE} (-p_u \sin\theta + \tau_u \cos\theta) ds_u + \int_{LE}^{TE} (p_l \sin\theta + \tau_l \cos\theta) ds_l \qquad (1.10)$$

By using Eq. (1.3) and (1.4) corresponding lift and drag values can be calculated. However, in order to be able to compare different airfoils, dimensionless forms of aerodynamic forces much more handful.

$$P_d = \frac{1}{2} \rho_\infty V_\infty^2 \qquad (1.11)$$

Equation (1.11) is called *dynamic pressure*. In order to drive dimensionless coefficients, forces and moments are divided with dynamic pressure since it is the only form of pressure that is a function of the velocity[27].

$$C_L = \frac{L}{P_d S} \qquad (1.12)$$

$$C_D = \frac{D}{P_d S} \qquad (1.13)$$

In equations (1.12) an (1.13), lift and drag forces are of a whole wing, where S is the total wing area. Same formulations are also applicable to normal and axial forces.

$$C_N = \frac{N}{P_d S} \qquad (1.14)$$

$$C_A = \frac{A}{P_d S} \qquad (1.15)$$

And the moment coefficient is:

$$C_M = \frac{M}{P_d S} \qquad (1.16)$$

While calculating for airfoils, some modifications should be carried out on the equations. An airfoil is the representation of a wing section for unit span length. Therefore, forces acting upon the airfoil profile are per unit length. This difference reveals itself when choosing the characteristic length for the equations as well. For airfoil correlations, characteristic length is the *chord length c*.

It is possible to drive calculations for airfoils by modifying equations (1.12),(1.13) and (1.15).

$$c_l = \frac{L'}{P_d c} \tag{1.17}$$

$$c_d = \frac{D'}{P_d c} \tag{1.18}$$

$$c_m = \frac{M'}{P_d c} \tag{1.19}$$

Equations (1.17),(1.18) and (1.19) are lift, drag, and moment coefficients for airfoils respectively.

CHAPTER 2

MODEL AND METHOD

2.1. Simulation Process

Proposed design in this study is to create a relatively hotter fluid layer on the swept area of the wing. This thin fluid layer can prevent ice formation by acting as an insulation film. In order to achieve this, small openings have to be placed on the swept surface of the wings. As the wind flows over turbine blades, it creates a suction and supplied air (relatively hotter) naturally covers the surface of the wing. Supplied air can be taken from surrounding of any element of turbine that generates excessive heat. A representative figure of the proposed design can be seen below.

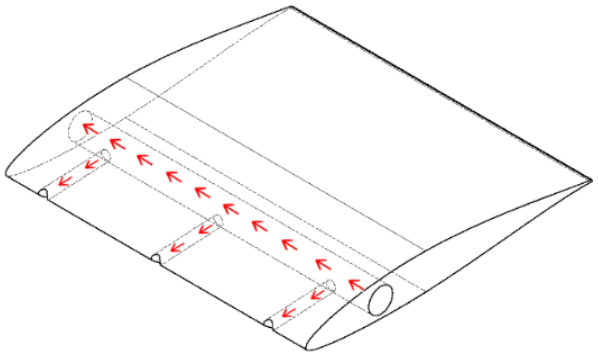

Figure 17. Representative figure of the proposed design

Purpose of this study is to find optimum values for design parameters of the mentioned solution and testing scenarios with numerical models. The main concern is to preserve the lift as much as possible. Even though it is already foreseen to have some loss in the lift, overall operation efficiency can be increased since there will be no need for maintenance related to ice formations.

In order to investigate fore-told phenomena in detail, establishing a proper model is a necessity. There are several aspects to be considered while preparing a simulation model of any kind of physical and/or chemical event that is of interest. Those aspects are

not exactly simulation steps but more general inclusive categories. They can be dismantled into the following segments:

- Method
- Mesh
- Post-process

The method is, in fact, a broad section. Geometry, and how it is handled, also the way simulation is established (including decisions about boundary conditions and assumptions) directly go into this part. Method part is namely the planning part of a simulation.

To be able to start the simulation process, related physics/governing equations of the problem should be studied extensively. Otherwise, it would be the most hopeless to expect meaningful results from the simulation, because at the very beginning the problem is not defined accurately. Also, knowledge of physics behind the problem allows one to use adequate assumptions. So that, computational power requirements may be lessened by a noticeable amount. One of the expertise requiring parts of a simulation, most of the time, is the knowledge about applicable assumptions according to the case. In this study's case, instead of modelling the whole wing of the wind turbine, just a partition is used. How it is possible and gives useful results is explained in the following sections in details.

Choosing a model for the problem is another vital point to be considered. There might be different ways of solving the problem numerically. Each represents a different "model"; a different mathematical approach to tackle down the problem. Most of the time, each of those models have their own strong and weak points compared to each other. It does not mean a model is superior to another just because there is a complexity difference between them in terms of mathematical expressions. It is their capability of solving the problem that matters in different cases.

In all simulations during the study, Shear-Stress Transport (SST) k-ω model was used in all simulations during the study. The main reason for this is that the performance of the k-ω model is better than the k-ε model if any separation is observed[28]. Since energy equations are also used in simulations, the solution of the boundary layer has become more important. Therefore, using SST k-ω model is more suitable since it is a combination of k-ε and k-ω models. SST k-ω model combines the robust formulation of k-w near the wall region with freestream independence of the k-ε model away from the walls.

The general form of mass conservation and momentum conservation equations solved by ANSYS Fluent are given as below[28].

$$\frac{\partial \rho}{\partial t} + \nabla \cdot (\rho \vec{v}) = S_m \tag{2.1}$$

Equation (2.1) is the general form of mass conservation that is valid for both incompressible and compressible flows. S_m is identified as the mass added from the second dispersed phase to continuous phase, and any user-defined source.

$$\frac{\partial}{\partial t}(\rho \vec{v}) + \nabla \cdot (\rho \vec{v} \vec{v}) = -\nabla_P + \nabla \cdot (\bar{\bar{\tau}}) + \rho \vec{g} + \vec{F} \tag{2.2}$$

The general form of momentum conservation is given in equation (2.2) where p is the static pressure, $\bar{\bar{\tau}}$ is the stress tensor, $\rho \vec{g}$ is the gravitational body force, and $\vec{F}$ is the external body force. Also, effects of porous-media and any user-defined sources are introduced with the $\vec{F}$ [28].

The stress tensor $\bar{\bar{\tau}}$ is given as it is in equation (2.3).

$$\bar{\bar{\tau}} = \mu \left[(\nabla \vec{v} + \nabla \vec{v}^T) - \frac{2}{3} \nabla \cdot \vec{v} I \right] \tag{2.3}$$

In equation (2.3), the second term on the right-hand side is the effect of volume dilation, μ is the molecular viscosity, I is the unit tensor.

The energy equation solved in ANSYS Fluent is in the following form:

$$\frac{\partial}{\partial t}(\rho E) + \nabla \cdot \left(\vec{v}(\rho E + p) \right) = \nabla \cdot \left(k_{eff} \nabla_T - \sum_j h_j \vec{J_j} + \left(\bar{\bar{\tau}}_{eff} \cdot \vec{v} \right) \right) + S_h \tag{2.4}$$

The first three right-hand side terms of Equation (2.4) energy transfer due to conduction, species diffusion, and viscous dissipation. S_h includes the heat from chemical reactions, any other volumetric heat source defined by the user. In the energy equation, k_{eff} is the effective conductivity, and J_j is defined as the diffusion flux of species j [28].

Mesh is another critical part of a simulation. In fact, one might say it is the trickiest one in terms of getting good results. Overall, in most of the simulation software what is done is solving the problem by dividing the problem domain into smaller partitions.

Therefore, representing a division of a physical domain of a problem with essential features is a demanding task. Also, some metrics of a mesh directly related to the capability of a model, or even the success of a solver. A nice example would be the difference in requirement of k-ω and k-ε models in terms of y+ of boundary layer mesh. While the k-ε model is able to solve a CFD problem with y+ values around 30 to 100, because of the difference in the theoretical background of the models, k-ω requires a boundary layer mesh with y+ close to 1. Basically, generating good and adequate mesh is important as much as setting up the right model.

Importance of post-process part comes from the very beginning of the problem. Post-process is where data of the results are evaluated. Therefore, one must know what to look in a crowded data. Because, if the parameters to look for is not clear, then there is no need for the simulation at the very beginning. Simulating a physical event in a digital environment, it is more than calculating values. In the most basic way, simulations do not work like calculators. In order to get meaningful results, the fine-tuning of a model is required. Thus, one needs to know what to look for in a problem, in order to understand, evaluate, compare and comment on the results.

2.2. Simulation Methodology

After describing the importance of aspects to be considered in a simulation, it is the most beneficial to break down the simulation methodology of this study.

In this section, simulation methodologies followed for the whole study is portrayed. Starting from geometric decisions to mesh parameters, and qualifiable results, all steps are explained in detail. At this point, it is possible to handle simulation methodologies in two separate parts. The first one is to build a valid model, the second one is where the thermal performance of the proposed design is studied by using the validated model.

2.3. Geometry

Generating a geometry for this study started with picking up an airfoil for the problem. Selection of the airfoil is important since it is a pure numerical study. And if there are no data to compare the results of the simulations, validation of numerical results

would be impossible. In such a case, results might end up being useless. Therefore, S830, an airfoil profile recommended by NREL for the primary section of a wind turbine with 30 to 40 m rotor diameter is selected.

It is being recommended for the primary part of a wind turbine, enables us to apply certain assumptions without worrying much. Turbine blades have some certain geometric features at the base/root and the at the tips. In most of the designs, sharp twists are introduced close to the base. Also, many designs have a part called “spoiler” close to the base. That is some sort of extension part. At the tip, taper ratio changes such that, the cross-section area of a turbine blade decreases drastically. Other than that, most of the wind turbine blades have a curved cap with the purpose of reducing tip vortices. Therefore, choosing an airfoil design for the primary part reduces the number of critical points to be considered.

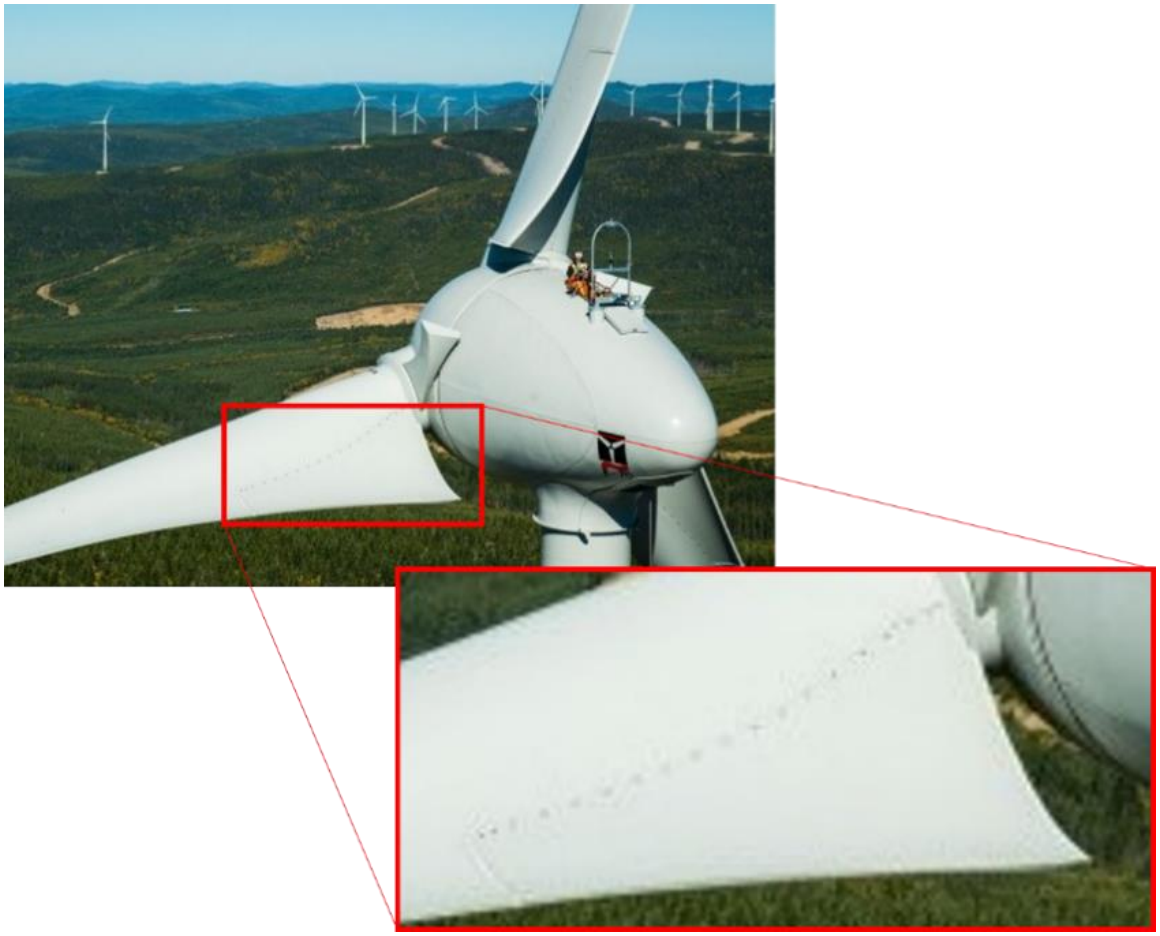

Figure 18. Wind Turbine Spoiler(Source:[29])

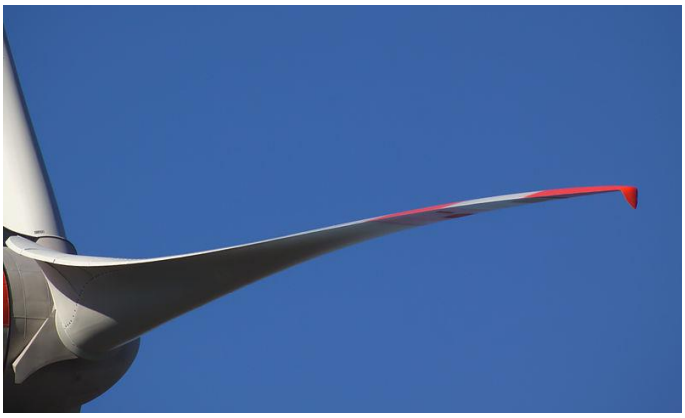

Figure 19. Wind Turbine Blade Tip (Source:[30])

One of the main assumptions in this study is neglecting the influence of induced velocity. Since prevention of phase change conditions in the boundary layer around the airfoil is investigated, the simulation models are focused more on the detailed results inside the boundary layer. Therefore, it would require too much computational power to solve the whole turbine blade. Instead, using a portion of it is much efficient in terms of meshing, solving and post-processing time.

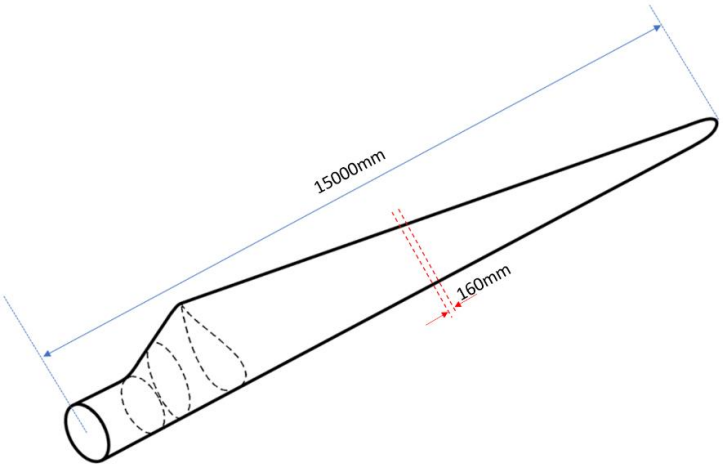

Figure 20. Representative section view

As can be seen in the representative figure above, a simplification of taper ratio is sensible, since the maximum width of the section in this study is set to 160 mm. The rotor diameter of wind turbines suggested for S830 airfoil is 30~40 m. With a loose calculation, assuming blade length as 15m, 160mm section is roughly 1% lengthwise. Therefore, it is safe to neglect geometric changes due to the taper ratio, and the assumption of constant chord length is legit.

Another reason to only pick a section of a blade is to be able to calculate the optimum distance between each port on the wing. In theory, the width of the thermal boundary layer projection on the wing surface directly gives the optimum distance between two openings, as it shows the thermally active region.

Solving for only a partition of a wing is possible by applying symmetry boundary condition to both sides of the wing. However, if symmetry is active at both side, then now this small section turns into a partition of an infinitely long blade with no taper ratio. So, all aerodynamic properties of this element are independent of its position on the blade. At this point, calculations for the finite wings are not conclusive; it is airfoil equations that are valid.

2.3.1. Geometric Operations

The first operation is to generate airfoil shape. After generating the closed surface of the airfoil S830, extrusion is applied. The depth of the extrusion is one of the parameters that are essential in this study. Therefore, it is not given an absolute value, instead, it is kept as a parametric entry for the model.

Simplifying geometries while at the pre-process of a simulation is a quite common methodology. It is simply removing geometric features that give complexity to the mesh but not the problem itself. Removing design details similar to chamfers and fillets is a good example for these operations. Time to time, such geometric alterations are carried out in order to prevent problems regarding mesh phase. In most of the cases, chamfers and fillets are small design features. As a feature gets relatively smaller, in order to be able to represent it in mesh form, if otherwise is not commanded, meshing algorithms scale down element size. This situation results as an increase in solution time for the simulation, which is not desired at all. However, in some cases, a chamfer or a radius is introduced. The main reason for that is to eliminate a problem called “Self-proximity”. Self-proximity occurs when the angle between the two converging faces is so small. Also, this narrow path retains the boundary layer mesh to grow in between. Therefore, it is safe to say geometric modifications are very situation dependent.

In this study, in order to be able to grow the boundary layer mesh without a problem, a fillet of 0,1mm is introduced to the tail of the airfoil profile. This revision allowed the boundary layer mesh to grow without any problem. Dimensions of the tunnel geometry are given in the following figure.

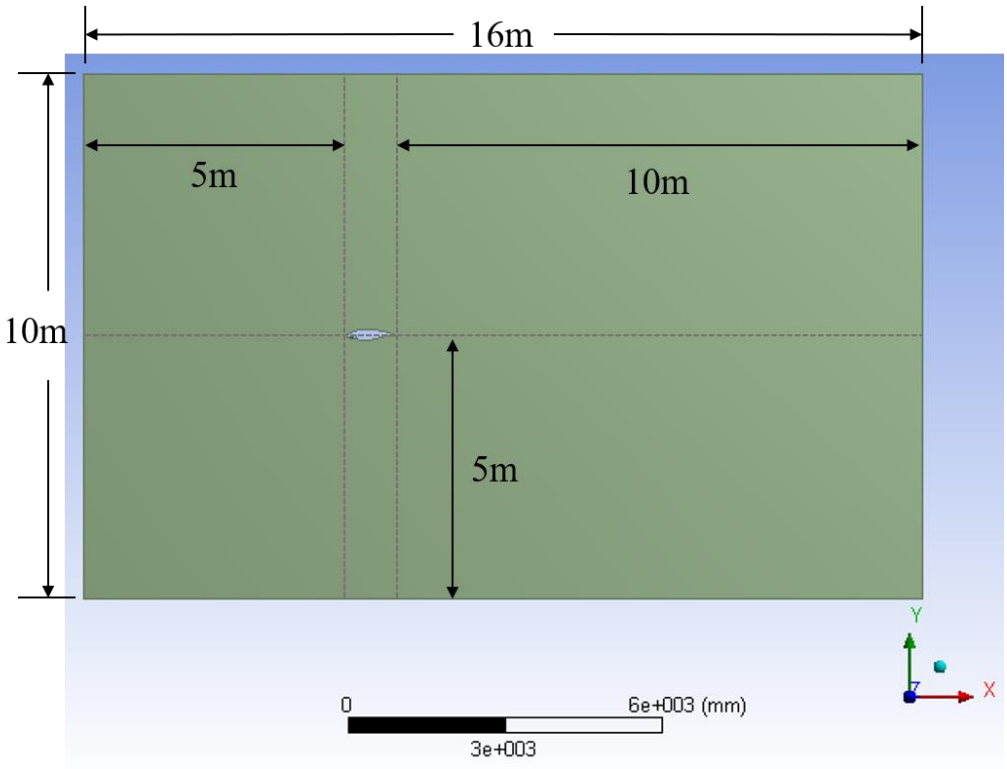

Figure 21. Tunnel dimensions

In order to have a parametric study, some dimensions are set as variables that change for every design iteration including orientation of the blade section inside the wind tunnel. One might defend the convenience of altering velocity components instead of changing the angular orientation of the blade section and meshing it every time. Most of the time it really is more convenient to change velocity components. However, in the case of this study, it is not quite applicable because of a simple reason. Firstly, in order to get rid of the effects of backflow, tunnel geometry should be long enough before and after airfoil geometry. This means a quite long flow domain compared to the chord length of the airfoil. When velocity components are given at the inlet of the tunnel, velocity profile changes in such a manner that it will not have any vertical component as it used to have at the beginning. It lets the airfoil to face completely different velocity and pressure field than the intended.

When it comes to the cases studied, the parametric chart below had been followed in Table 1. This cases repeated at angles of attack of -6, -3,0,3,6 degrees. All the parameters selected as linear products of the chord length.

Table 1. DoE Table of the simulation cases

c - Chord length(mm)	**d – Pressure inlet diameter(mm)**								
1000	**d=0,02×c**			**d=0,03×c**			**d=0,04×c**		
	20			**30**			**40**		
	Width (mm)			**Width (mm)**			**Width (mm)**		
β Angle (Degree)	**2d**	**3d**	**4d**	**2d**	**3d**	**4d**	**2d**	**3d**	**4d**
-2	40	60	80	60	90	120	80	120	160
0	40	60	80	60	90	120	80	120	160
2	40	60	80	60	90	120	80	120	160

2.4.Mesh

Mesh process is mostly where trade-offs happen. As size per element decreases, one can capture simulation domain in a more detailed manner. However, more details mean a higher number of mesh elements. It is important not to forget that each mesh element is the small piece of the simulation domain to be solved. In other terms, the computer solves governing equations of the problem for each element. More mesh element means more computational power, and/or more memory requirement, and/or more computational time. It is important to generate a well-balanced mesh. The most detailed mesh does not always mean a better mesh. There are several sides to the story other than just size. A good mesh can be described as just sensitive enough to capture details of physics accurately and precisely, and costs low in terms of computational power both during the meshing and solving processes.

A manually operated meshing process gives freedom to the user most of the time because it gives the opportunity of controlling over every mesh element in terms of sizing, density and quality. It is especially good if all the critical and noncritical points of the model are known. So, the mesh domain can be modified to correspond to the local requirements of the physics. While increasing density and decreasing size at some point, doing the exact opposite at another point might lead to compensation at the number of total mesh elements. Thus, steers to getting relatively more adequate setup to acquire results without increasing number of mesh elements much.

2.4.1. Meshing Operations

As unravelled in preceding discussions, meshing is a trade-off between desired depth of detail and computational power and/or time. Mostly, the computational part of this trade has its roots bounded up directly to a cost. The cost, in this case, might be a literal amount of money required to buy certain hardware to be able to solve the problem, or the time required to complete simulation runs. Therefore, finding an optimum mesh is important. Since a high-end workstation was not available, local sizing operations were highly needed, and moderate mesh sizes were inevitable.

As can be seen Table 1., the smallest feature aside from surface partitions on the airfoil is the pressure inlet pipe. Therefore, the minimum element size is selected to capture this geometric feature in enough detail. The very nature of the simulation scenario in this study requires a large wind tunnel geometry, because of such requirement, local sizes are given to certain regions. Sizing of mesh elements gradually increases as one gets further from the airfoil. The boundary layer is the most critical mesh sector in the whole model. It is covered by a special boundary layer meshing method. Then, there is an offset zone of 50 mm where mesh element size is 10 mm in the final models. It is also important to stress there is a strategic zone apart from the offset zone. This zone covers the most part of the higher-pressure gradients. Instead of meshing all geometry in great detail, having this certain region intensively meshed is an advantage in terms of meshing and solving time. The following figures present the foretold regions highlighted.

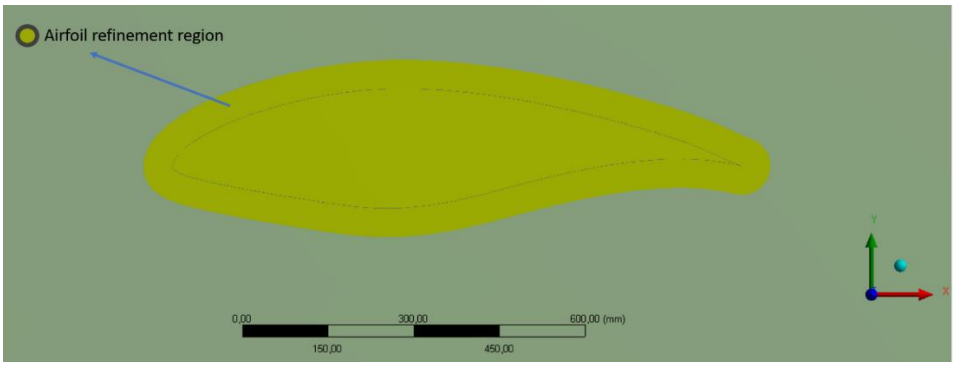

Figure 22. Airfoil mesh refinement region

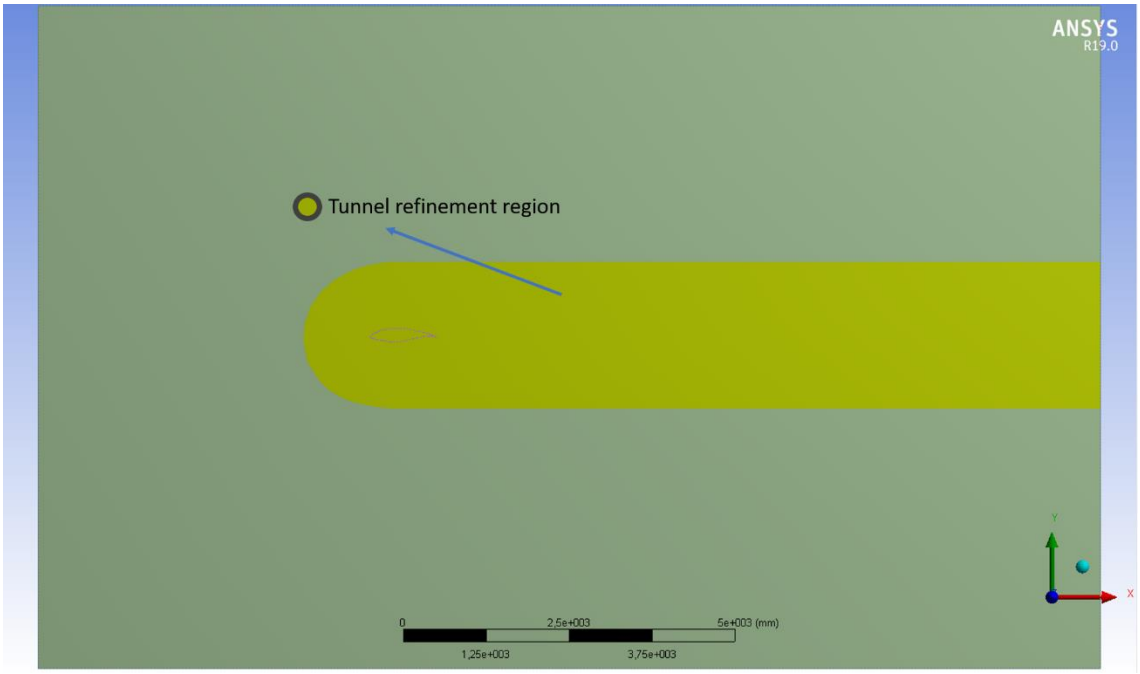

Figure 23. Tunnel mesh refinement region

2.4.2. Mesh Test

It is essential to know a model is not dependent on the mesh. Being dependent on mesh size, or in some cases mesh type, means getting different results for each mesh tryout. This is certainly unwanted.

In order to prove that results of a model are free of mesh parameters, a mesh independency test is required. This test is merely trying different mesh options, mostly from a relatively coarse mesh to finer meshes. By executing this, it is also possible to find an optimum mesh size for the model.

In the present study, a few mesh tests were carried out. The first one is to understand the general response of the model against changes in the mesh element size. At this point, the number of total elements is also important because of the limited computational power. Since the model is established with different multi-regional size control inputs, inserting differentiating values to those parameters would result in a small design of experiment table. And the following table gives selected values for sizing parameters in mm.

Table 2. Mesh independence table

Mesh Independence				
Design Point	**AoA (Degree)**	**Tunnel Ref Size(mm)**	**Foil Ref Size(mm)**	**Re Number**
DP0	0	100	10	4M
DP1	0	75	10	4M
DP2	0	50	10	4M
DP3	0	25	10	4M
DP4	0	100	5	4M
DP5	0	75	5	4M
DP6	0	50	5	4M
DP7	0	25	5	4M

Table 3. Mesh independence results

Mesh Independency				**Reference c_l**	0,71	**Reference c_d**	0,012723
Design Points	**Mesh Elements**	**Lift(N)**	**Drag(N)**	**c_l**	**Error%(Lift)**	**c_d**	**Error%(Drag)**
DP0	223960	96,3000	1,8612	0,656016181	7,60%	0,012678892	0,35%
DP1	262060	94,5070	1,8554	0,643801882	9,32%	0,012639381	0,66%
DP2	353950	93,5910	1,8509	0,637561894	10,20%	0,012608726	0,90%
DP3	1336000	93,9430	1,8390	0,639959793	9,86%	0,012527661	1,54%
DP4	1052700	91,1000	1,8426	0,620592669	12,59%	0,012552185	1,34%
DP5	1089700	90,8770	1,8493	0,619073546	12,81%	0,012597827	0,98%
DP6	1182200	91,1070	1,8179	0,620640355	12,59%	0,012383923	2,67%
DP7	2161000	90,8250	1,8100	0,618719311	12,86%	0,012330107	3,09%

For all eight runs, boundary layer mesh parameters are constant at a total thickness of 2 mm with 20 layers inside. Therefore, dependency results can be considered solely the function of the refinement sizes. A more useful representation of each case is compared in the graph below.

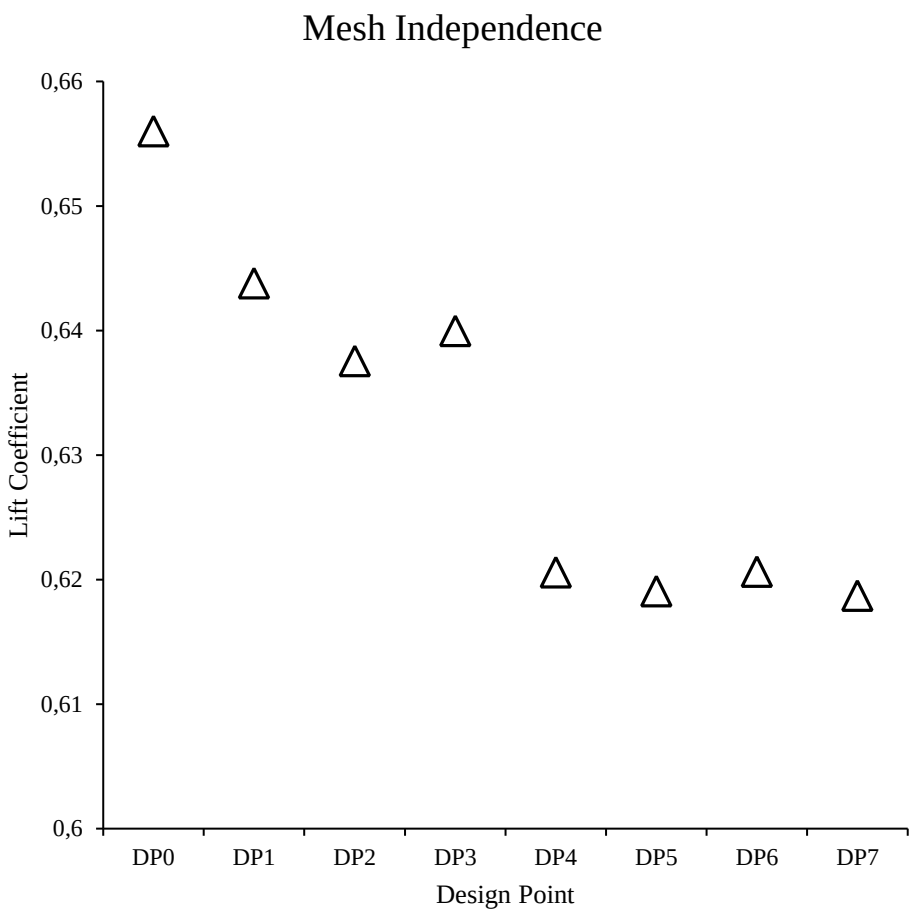

Figure 24. Mesh independency test results

Considering this model includes symmetry boundary conditions to represent an airfoil in 2D, each sizing is promising, with the maximum relative error to experimental results of 12,86% for lift and 3,09% for drag coefficients.

From Figure 24, design points DP2 and DP4 are reasonable choices for further investigation since they have enough depth in terms of mesh resolution, and number of elements. At this point, a more extensive mesh test is carried out for both cases. The previous test was to understand if the selected range of sizing parameters are adequate for the model, the second test is to see if these meshes can represent the general characteristic of the selected airfoil S930. In order to see such a response from the model, angle of attack is set as a variable parameter ranging from -6 to +6 degrees by 3 degrees of change. This means five different operating points for each case. Results are as it follows.

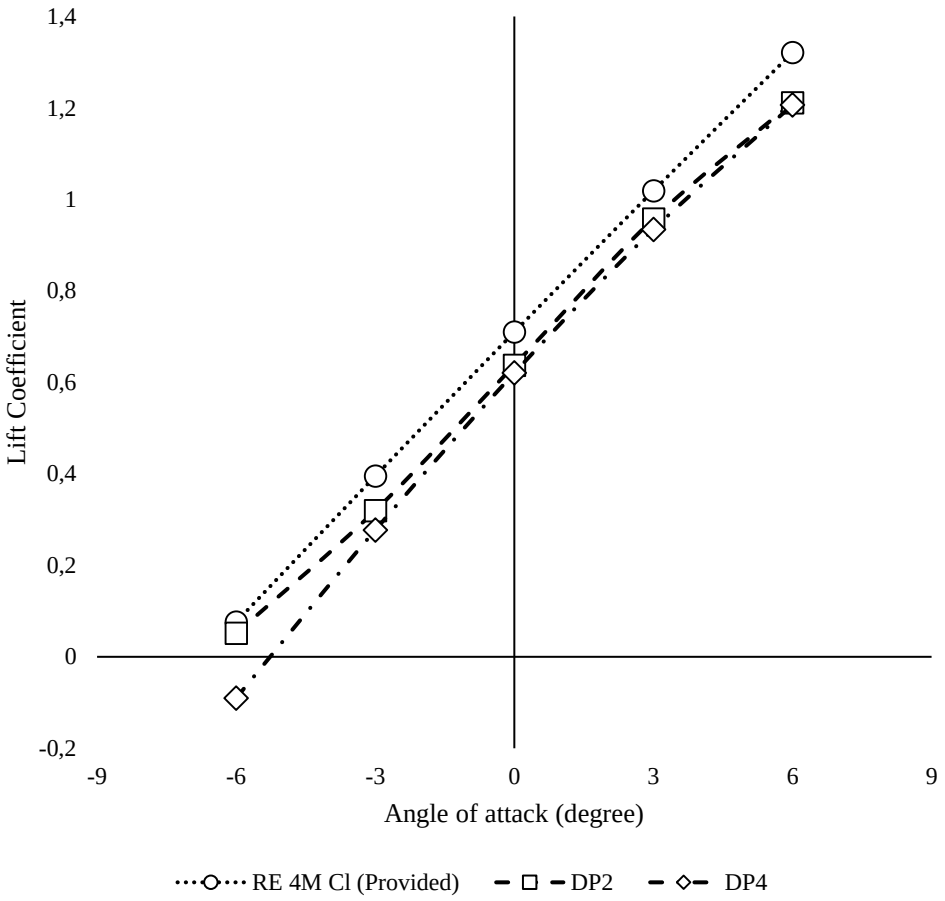

Figure 25. Comparison of mesh sizes

From this comparison, it can be deduced that design point DP2 is the optimum one to pick for tunnel mesh sizing, considering representing general aerodynamic performance and computational power requirement. However, it is a known fact the boundary layer mesh itself has an overwhelmingly huge impact on the results of al CFD simulations. Since candidates for general meshing size are selected, the next step was is to decide on boundary layer mesh metrics. In previous runs, boundary layer mesh of 2 mm with 20 layers was used as a reference point, therefore selecting test values evolved close to these numbers. Both, changing number of layers for constant total thickness, and changing total thickness while holding the number of layers are applied to find optimum size selection for boundary layer mesh.

DP 2 and DP 4 are previously chosen design points. From DP to DP12, different values of the maximum thickness of inflation layers are introduced to the models. For the rest of the models, different numbers of inflation layer are employed to the total maximum thickness of 2mm.

Table 4. Inflation mesh trials

Design Point	AoA (Degree)	Tunnel Ref Size(mm)	Foil Ref Size(mm)	Number of Layers	Inflation Maximum Thickness (mm)
DP 2	0	50	10	20	2
DP 4	0	100	5	20	2
DP 5	0	100	5	20	1,75
DP 6	0	100	5	20	1,5
DP 7	0	50	10	20	1,75
DP 8	0	50	10	20	1,5
DP 9	0	50	10	20	1,25
DP 10	0	50	10	20	1
DP 11	0	100	5	20	1,25
DP 12	0	100	5	20	1
DP 13	0	100	5	15	2
DP 14	0	100	5	25	2
DP 15	0	50	10	15	2
DP 16	0	50	10	25	2

As a result, the total thickness of 2 mm with 25 layers inside gave the optimum solution when the number of mesh elements and relative errors of c_l and c_d values are considered together.

Table 5.Results of inflation mesh trials

Design Point	c_l	Error%(Lift)	c_d	Error%(Drag)
DP 2	0,6378701	10,16%	0,012612305	0,87%
DP 4	0,6205008	12,61%	0,012559926	1,28%
DP 5	0,6263298	11,78%	0,012281451	3,47%
DP 6	0,6292556	11,37%	0,011976094	5,87%
DP 7	0,6694401	5,71%	0,011916121	6,34%
DP 8	0,6886861	3,00%	0,011263287	11,47%
DP 9	0,6960048	1,97%	0,010896637	14,35%
DP 10	0,7046305	0,76%	0,010227767	19,61%
DP 11	0,6363024	10,38%	0,011571267	9,05%
DP 12	0,6392776	9,96%	0,011073268	12,97%
DP 13	0,6182135	12,93%	0,012715149	0,06%
DP 14	0,6166188	13,15%	0,012597509	0,99%
DP 15	0,6402451	9,82%	0,012692615	0,24%
DP 16	0,6495732	8,51%	0,012450076	2,15%

In order to see the overall performance of the selected mesh size operates adequately, five more cases are simulated with varying angle of attacks. Results are as it follows.

Table 6. Results of chosen mesh case

Design Point	**AoA (degree)**	**c_l**	**c_d**
DP 16	-6	0,04146151	0,02444022
	-3	0,29801391	0,01275037
	0	0,64957319	0,01245008
	3	0,93098138	0,01551413
	6	1,21254686	0,02058015

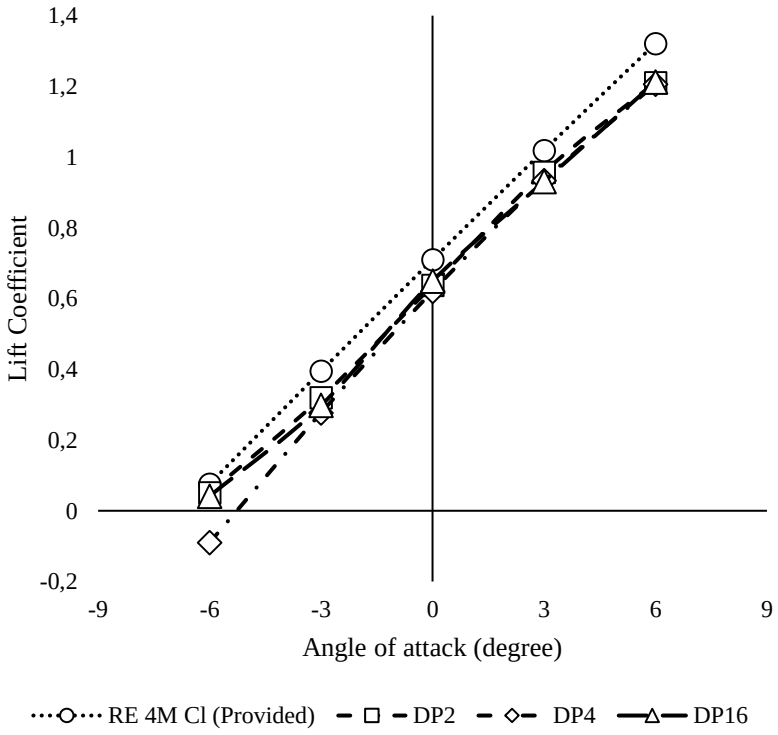

Figure 26. Comparison of lift output of the chosen mesh case

2.5. Thermal Model

The thermal model is established based on the validated model on previous topics. This time an inlet pipe, that would let air flow to the outer shell of the wing section, is introduced to the geometry. The newly introduced pipe is set as a pressure inlet to the model. By setting it as a pressure inlet, controlling flow rate and changes in the pressure field has become much easier. Instead of changing flow rates to catch a point where warmer air is just sliding over the wing, using local pressure values from previous models where the pressure inlet is positioned is more reasonable.

Every other aspect of the thermal model is the same with the model that has been used for validation of methodology, but the pressure inlet pipe. The main focus of this study is to understand how such an opening would affect the boundary layer and aerodynamic performance of the wing. Therefore, a design of experiment table is generated to form a frame for this study.

The only difference between the validated reference model and the thermal model is the addition of the pressure inlet pipe. The angle of this opening is defined by the clockwise direction from the chord line. Using this angle enables to see if there are differences in the pressure field and also aerodynamic efficiency to a large extent.

2.5.1. Thermal Simulation Cases

Under this topic, simulation cases regarding the subject of the study are explained extensively. As explained before, there are certain differences in the parameters of interest Therefore, knowing how all boundary conditions are cast into the problem is indispensable.

The airfoil data provided by NREL is for five different operating Reynold's Number; 2M, 3M, 4M, 6M and lastly 9M. As Reynold's Number changes for an airfoil with a constant chord line, the thickness of the boundary layer also changes. Therefore, simulation wise, different y+ values might be desired. But having different values of y+ for each Reynold's Number value requires repetition of mesh tests as well. Since this is a time-consuming process, choosing design Reynold's Number for simulations is a good reference point. Design Reynold's Number for S830 airfoil is stated as 4M by NREL.

The decision of the value at the pressure inlet is interpreted by using the reference models. It is possible to read pressure values on the walls of the airfoil profile, at the

pressure inlet location. Therefore, by using previous data, it is contingent to set a value to the pressure inlet; which would not be absurd in terms of operating conditions. What is desired is to have the fluid streaming from the pressure inlet to gently stick to the wall without facing any stagnation or without disturbing the pressure field abruptly. When it is achieved, it is possible to talk about a thin-film layer that would cocoon the surface and preclude it from ice accretion.

The value at the pressure inlet is set to 3000 Pa, which is greater than the average value taken from the reference model. If it is set to the average value directly, then the flow would be stuck in the pressure inlet pipe. That would cause the model to either diverge or give meaningless results. The temperature of the wind was set to 0ºC, and the temperature of pressure inlet was given as 20ºC.

In addition, a small set of simulations were run under conditions where the pressure input value was 2500 Pa, and the tunnel temperature was -10ºC to see the response of the system to different pressure and temperature values.

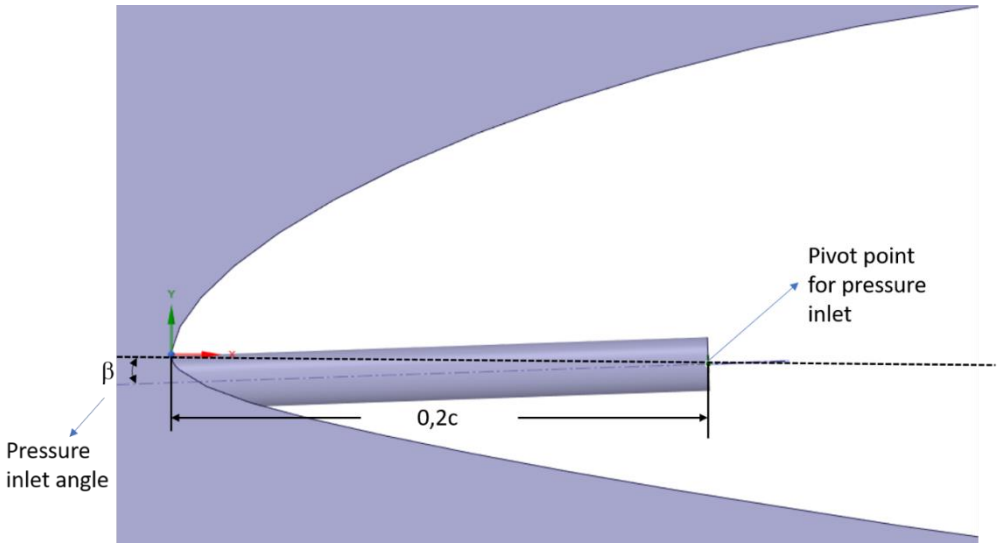

Figure 27. Pressure inlet angle, β

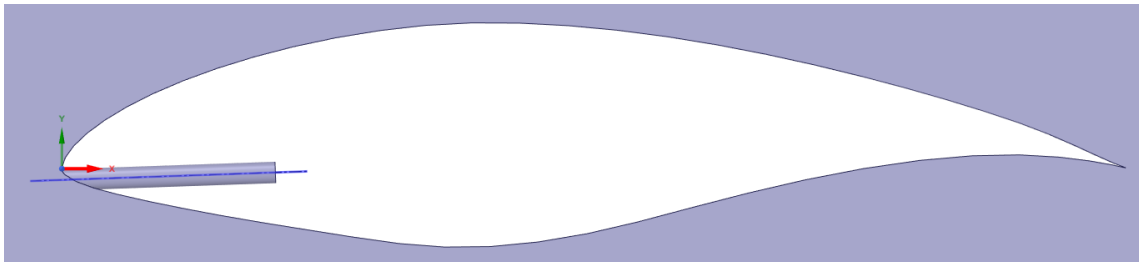

Figure 28. Side view of the geometry of the thermal model

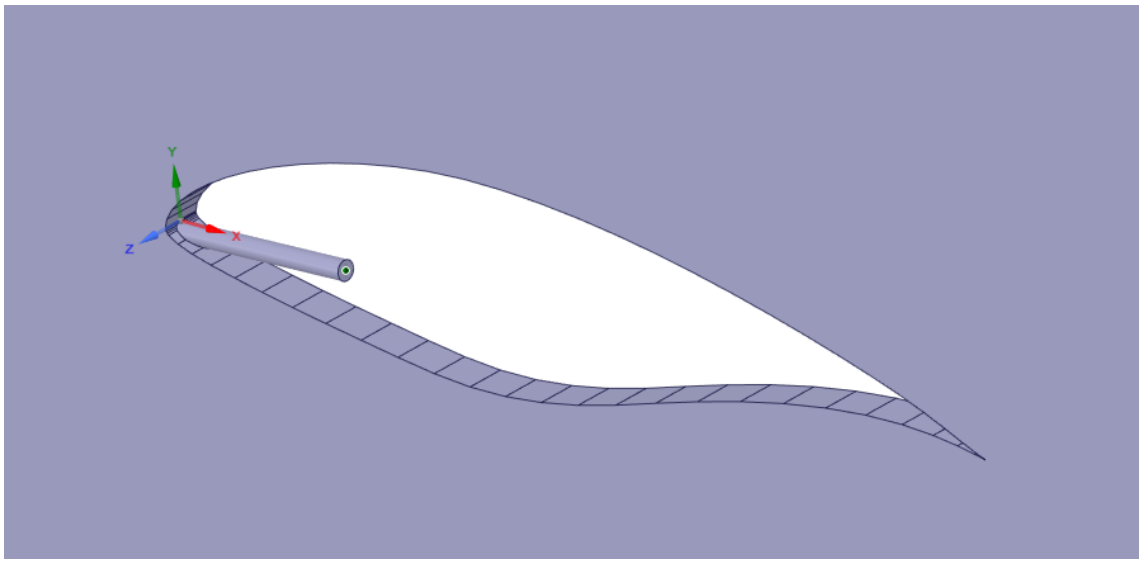

Figure 29. 3D view of thermal model with pressure inlet angle

CHAPTER 3

RESULTS AND DISCUSSION

3.1.Effect of Width/Diameter Ratio

In this study, basically, three different width/diameter ratios were examined. The openings of different diameters were compared with each other, and this comparison was repeated at different attack angles.

In all widths, it is possible to see that the effect of the large diameter span on the lifting force is relatively low when the angle of attack is below zero. The main reason for this is that when the angle of attack is below zero, the stagnation point moves along the upper surface of the wing profile, the flow out of the opening remains within the volume of flow separated from the tip zone and therefore does not have a large impact on the pressure field.

In most of the results, it is observed that designs having -2-degree angle create a relatively high lifting. At 0 and +2 degrees, the air coming out of the inlet of the pressure causes deterioration in the low-pressure area on the upper surface, thus causing more loss than the lifting force.

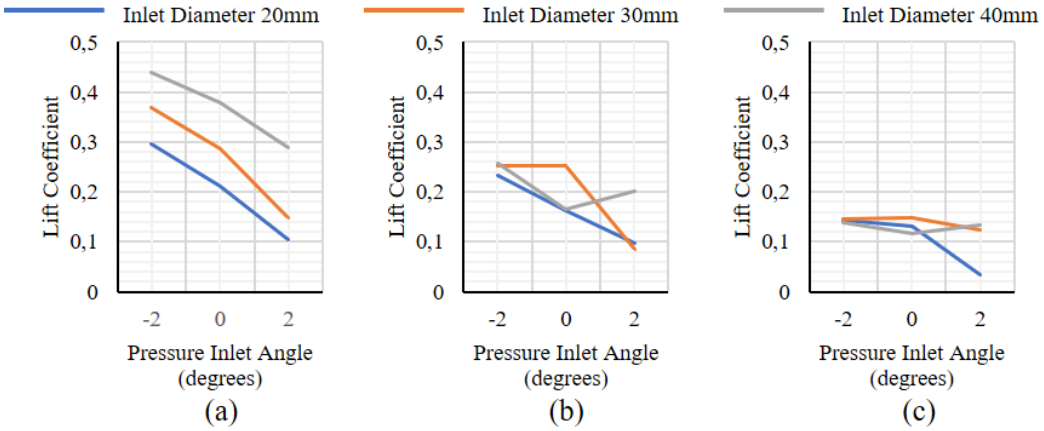

Figure 30. Effect of width/diameter at AoA=-6º, (a)Width=2d, (b)Width=3d, (c)Width=4d

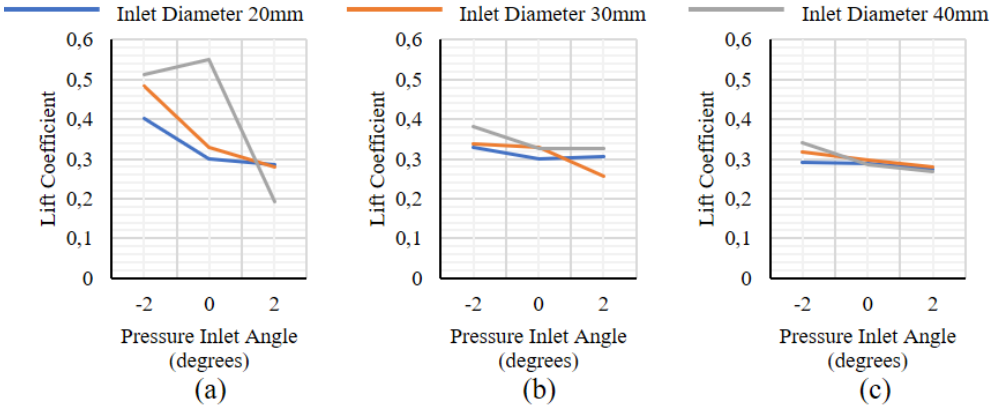

Figure 31. Effect of width/diameter at AoA=-3º, (a)Width=2d, (b)Width=3d, (c)Width=4d

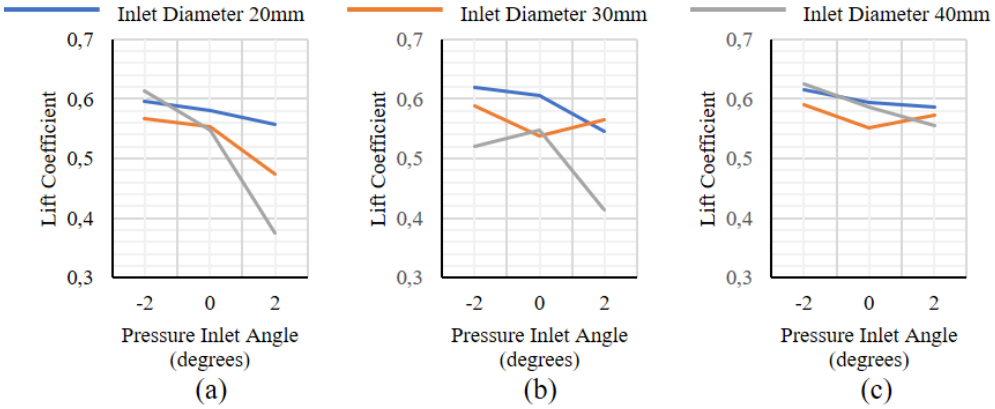

Figure 32. Effect of width/diameter at AoA=0º, (a)Width=2d, (b)Width=3d, (c)Width=4d

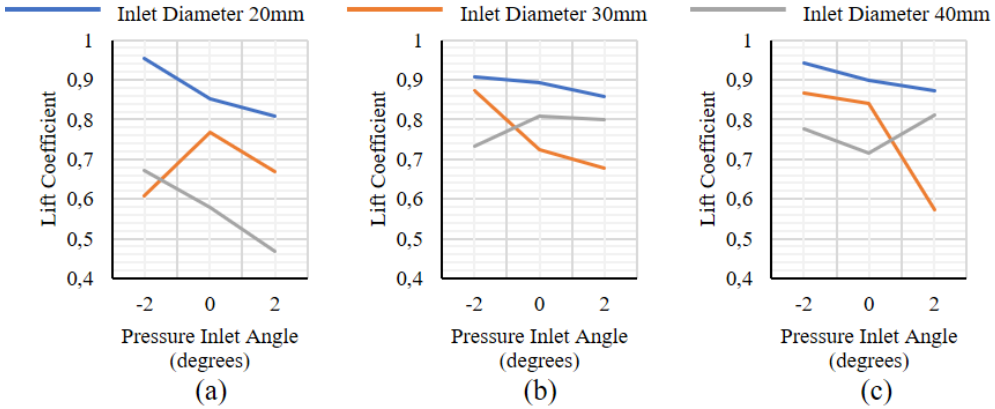

Figure 33. Effect of width/diameter at AoA=+3º, (a)Width=2d, (b)Width=3d, (c)Width=4d

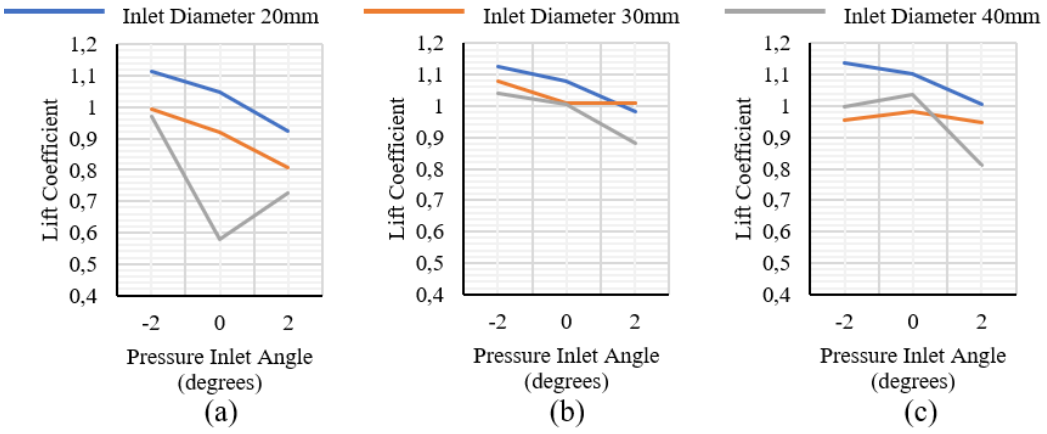

Figure 34. Effect of width/diameter at AoA=+6º, (a)Width=2d, (b)Width=3d, (c)Width=4d

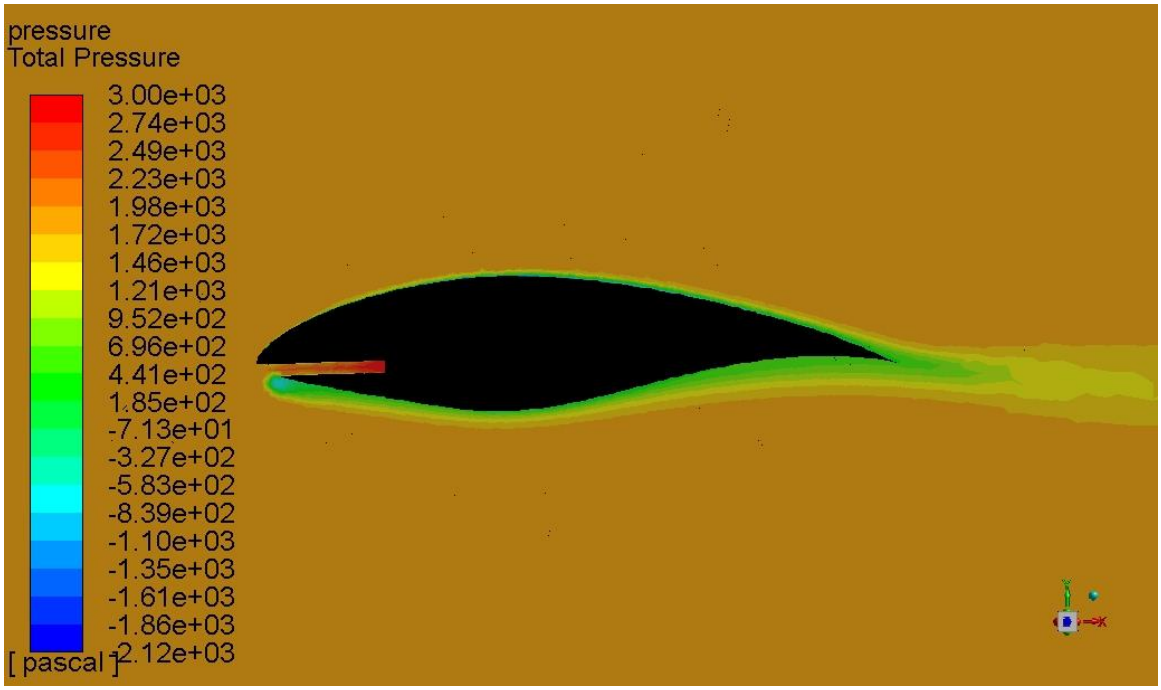

Figure 35. Pressure distribution at middle plane of the wing section, AoA=0º, Width=2d, β= -2º

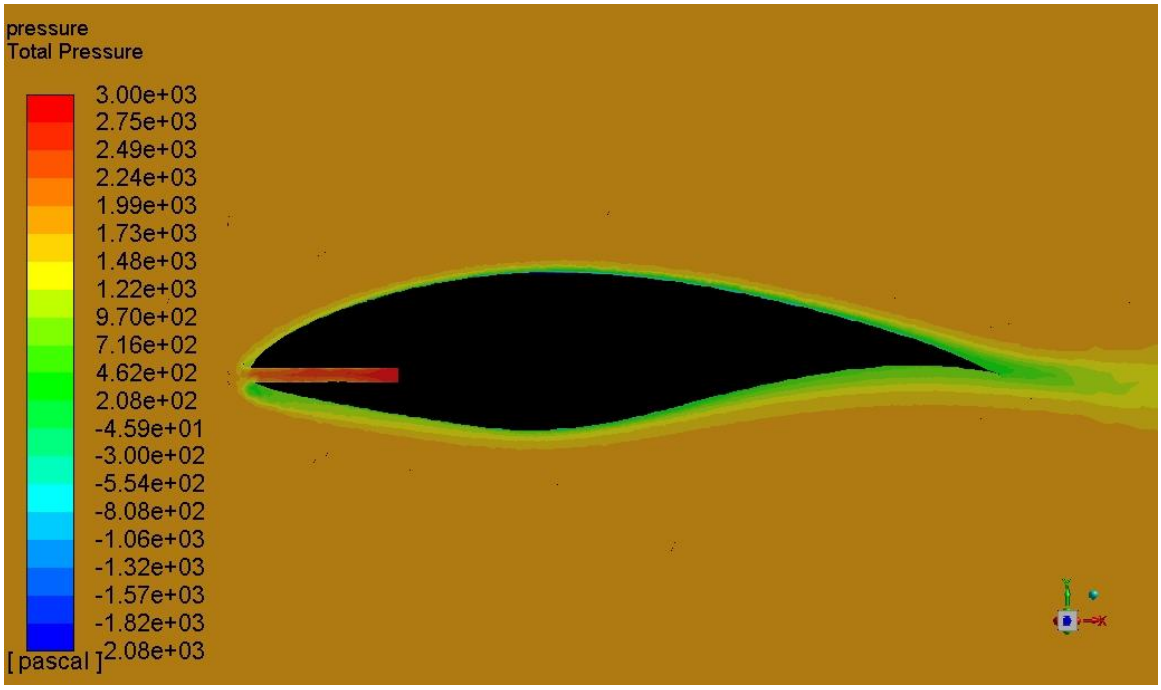

Figure 36. Pressure distribution at middle plane of the wing section, AoA=0º,

Width=2d, β= 0º

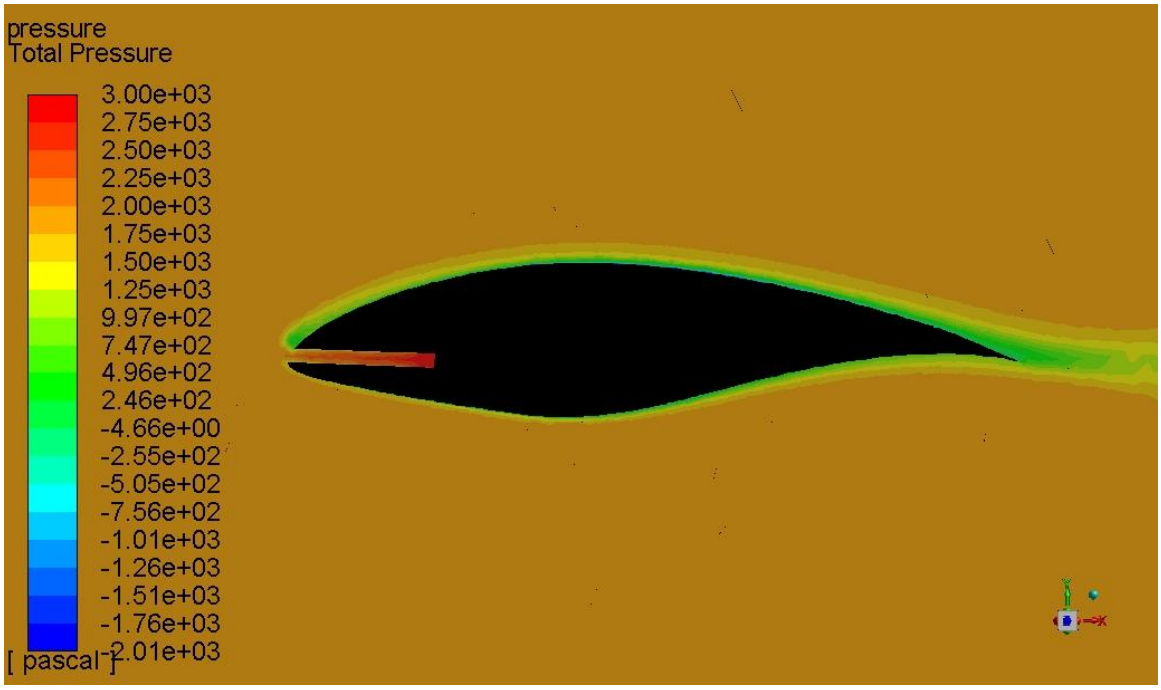

Figure 37. Pressure distribution at middle plane of the wing section, AoA=0º,

Width=2d, β= 2º

In Figures 35-37, the pressure distributions depending on the location of pressure inlet on three different positions are given. Even a slight change at the position of the pressure inlet at the tip of the airfoil changes the pressure zones.

In addition, when the width moves from 2d to 4d, the lift shows a more stable trend in all designs. The main reason for this is the reduction of the *d/w* ratio. Thus, a larger area of the wing section can meet the air without being influenced by the pressure inlet.

In order to see this effectively, it is useful to look at the results of the lifting force for each angle of entry and angle of attack on a fixed diameter. For this comparison, designs with 20mm diameter were chosen and the trend of the lifting force for all pressure inlet angles at each attack angle was examined.

As the graphs indicate in Figure38, as the *w/d* ratio increases, the tendency of the lifting force becomes more stable. As mentioned earlier, when the attack angles are -6 and -3 degrees, the effect of the pressure inlet on the lifting force of the wing tends to show the opposite tendency of when the angle of attack is greater than zero.

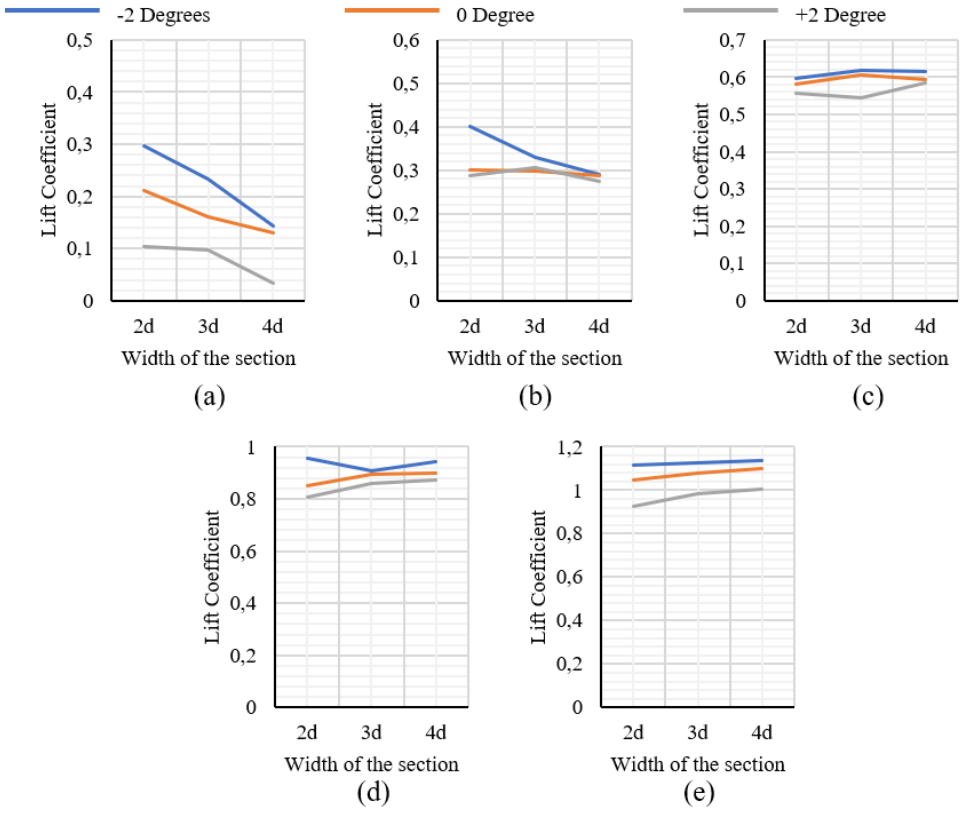

Figure 38. Comparison of pressure inlet angle on lift performance, (a) AoA=-6º, (b) AoA=-3º, (c) AoA=0º, (d) AoA=+3º, (e) AoA=+6º

3.2. Comparison of Lift Characteristics

In order to understand the influence of the pressure inlet on the overall performance of the wing section, each parameter set can be examined independently. This is only possible by comparing the parameters with the reference values in sets. This comparison is more useful for seeing the effect of the position of the pressure inlet on the characteristics of the lift, with a fixed width and a fixed diameter. The graphs for each diameter and width match are presented below.

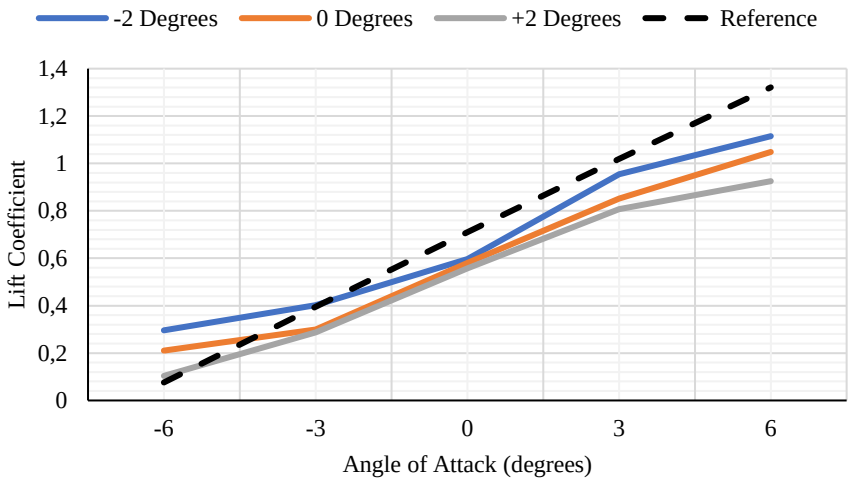

Figure 39. Diameter 20mm, Width 2d”

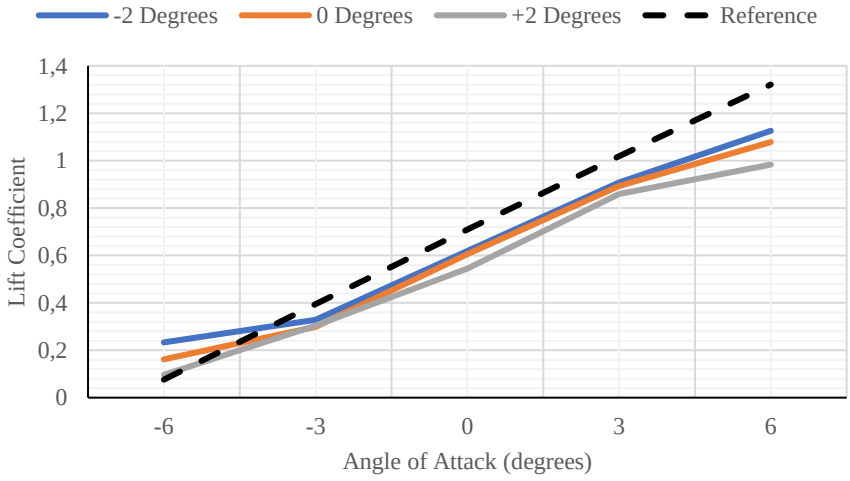

Figure 40. Diameter 20mm, Width 3d

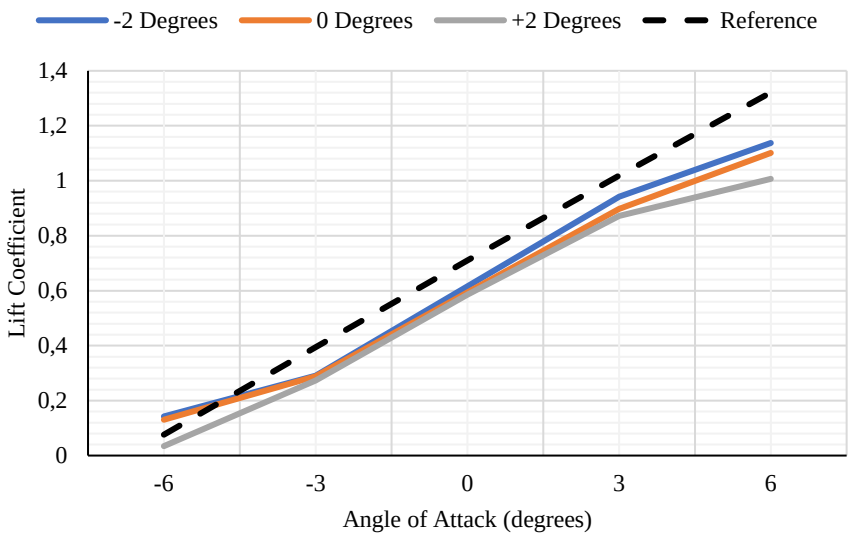

Figure 41. Diameter 20mm, Width 4d

Looking at the results, it can be observed that there is a general loss in lift force. In addition, the effect of the aforementioned *w/d* ratio can be clearly observed. As the ratio grows, the effect of the opening on the wing decreases, and the results approach the reference values. It is possible to see the same effect in other diameters. The following graphs are given for pressure inlet diameters of 30mm and 40mm.

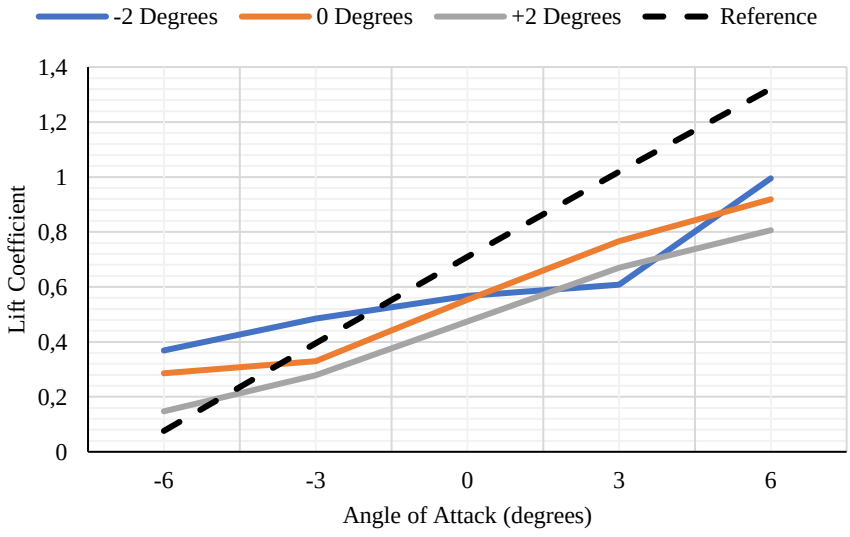

Figure 42. Diameter 30mm, Width 2d

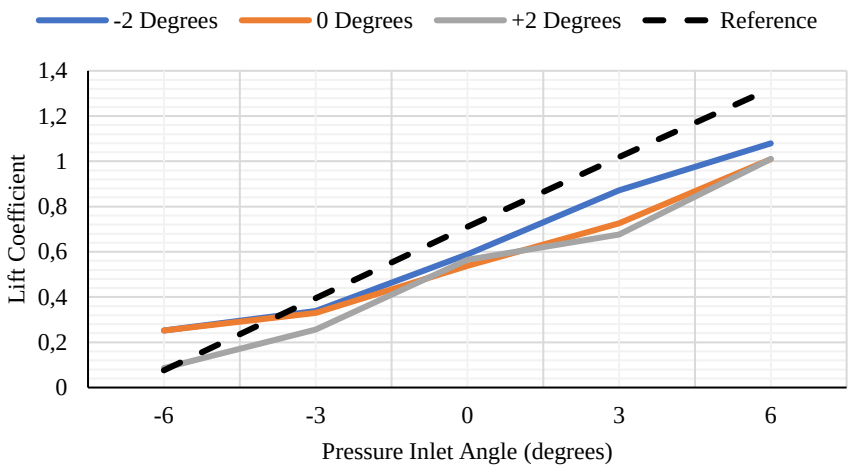

Figure 43. Diameter 30mm, Width3d

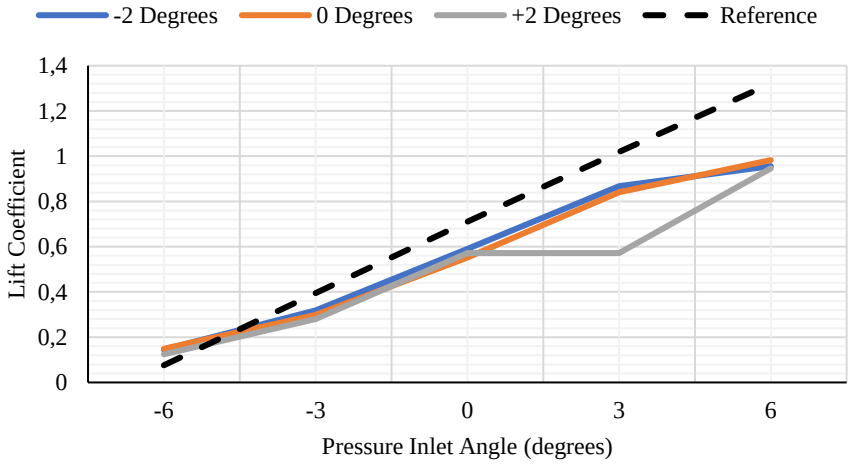

Figure 44. Diameter 30mm, Width 4d

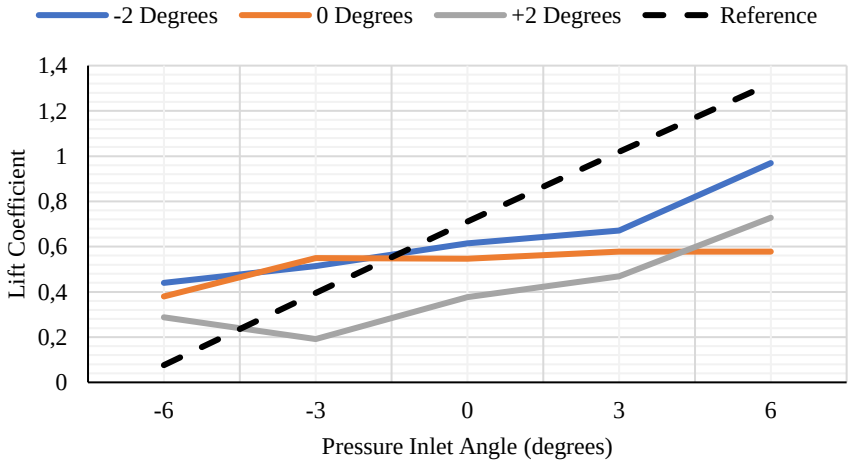

Figure 45. Diameter 40mm, Width 2d

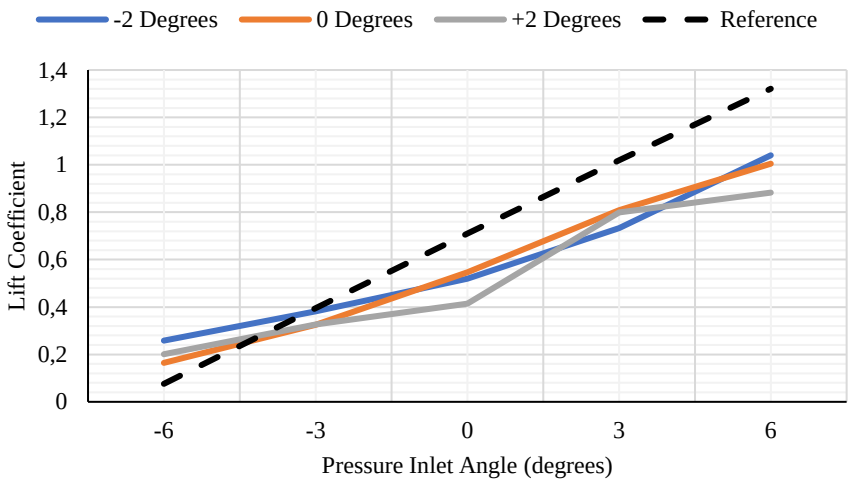

Figure 46. Diameter 40mm, Width 3d

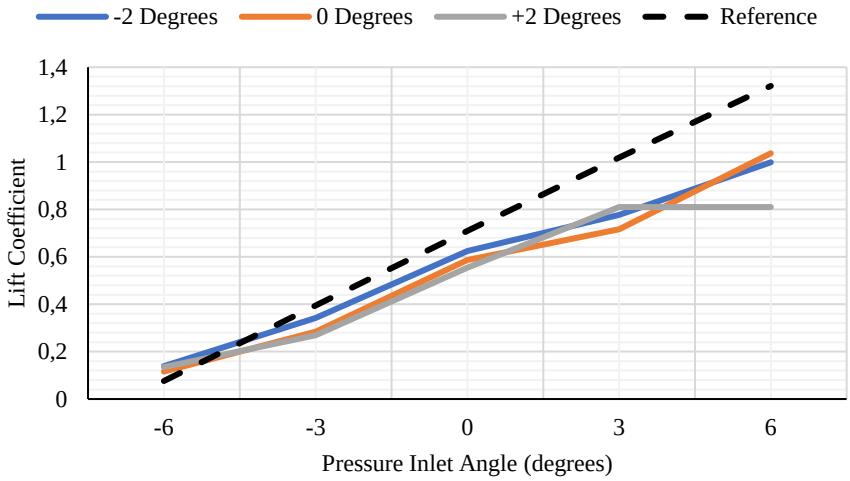

Figure 47. Diameter 40mm, Width 4d

Looking at the results of 40mm, which is the largest diameter of the data set, it is observed that as the w / d ratio increases, the general lift characteristic becomes more stable. Furthermore, when the angle of pressure inlet is considered in each case, it is observed that -2 degrees give relatively better results.

3.3.Surface Temperatures

The effect of the pressure inlet on the pressure area around the blade profile is described in the previous headings. Under this heading, it was examined how the film layer formed affected the surface temperature.

In Figures 35-37, it was observed that the hot air could not pass to the upper side of the wing while the angle of the pressure inlet was -2 degrees, and hot air directly moved towards to the lower surface. Of course, it is possible to talk about the exact opposite. As can be seen from the same figures, it is obvious that the hot fluid surrounds the upper surface at +2 degrees. And at 0 degrees, which can be considered neutral, the hot fluid is divided into the upper and lower surfaces.

This allows us to have an idea of how the temperature profile can be in the simplest way. As expected, the direction of the fluid on the blade directly affects the surface temperature as well as lifting performance.

Due to the fact that the hot fluid obviously switches between the upper or lower region with respect to the angle of the opening, an average temperature value taken from the entire wing surface will be misleading. For this reason, it is more accurate to separate the wing into the upper and lower parts by the leading and trailing edges and to look at the temperature averages separately on the surfaces. In the graphs below, while the attack angle is 0 degrees, the average temperatures of the upper and lower surfaces can be seen.

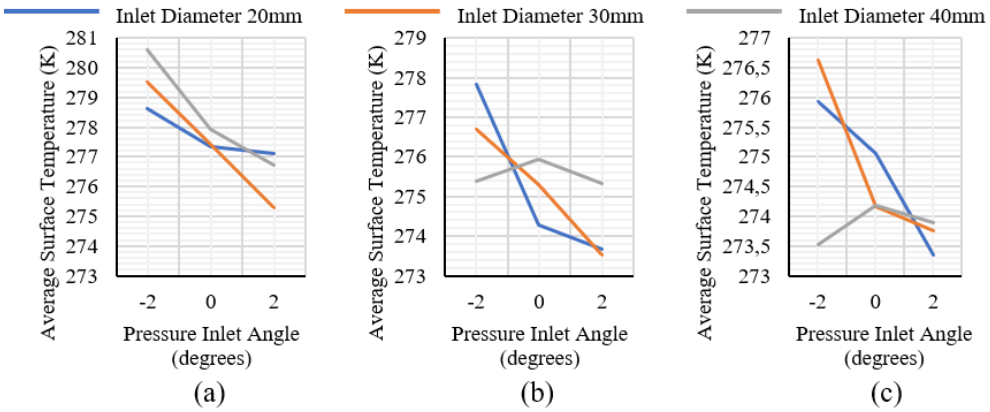

Figure 48. Lower surface, average temperatures, (a) Width=2d, (b) Width=3d, (c) Width=4d

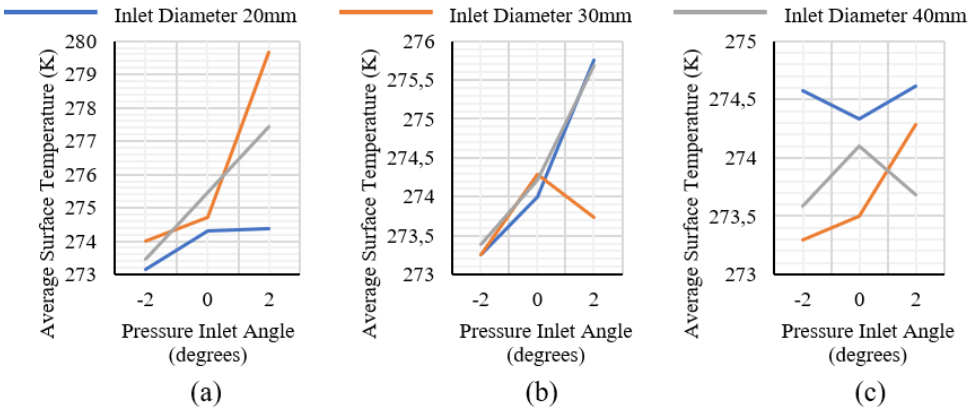

Figure 49. Upper surface, average temperatures, (a) Width=2d, (b) Width=3d, (c) Width=4d

When the temperature results are considered, it is possible to see that the temperature of the upper and lower surfaces show the opposite behaviour. Where the average temperatures of the lower and upper surfaces are closest to each other, as expected, the angle of the pressure inlet is zero degrees. In addition, it was observed that the average values of surface temperatures decreased depending on the width. The main reason for this is that the hot air leaving the pressure inlet does not sweep the wing surface over the entire width.

As described in the previous sections, studies in literature indicate that the icing starts from the tip of the wing. It has been observed that the pressure inlet can also cover the tip region with hot air at all three angle orientations.

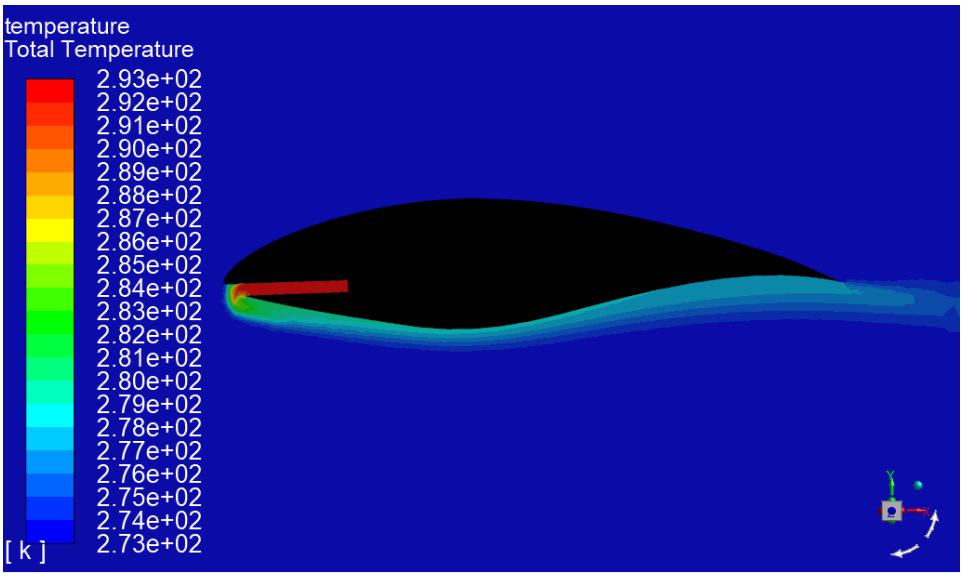

Figure 50. Temperature distribution at AoA=0º, β=-2º

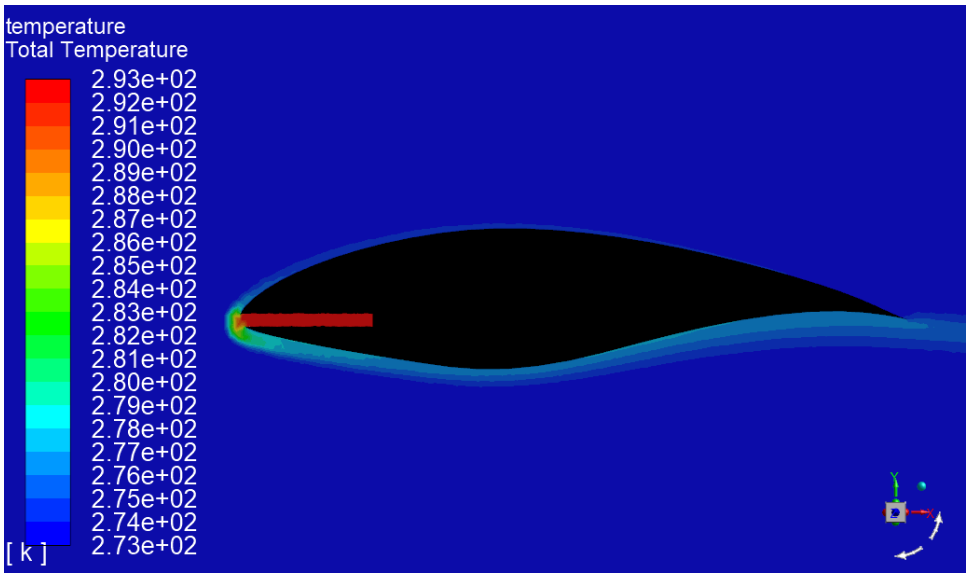

Figure 51. Temperature distribution at AoA=0º, β=0º

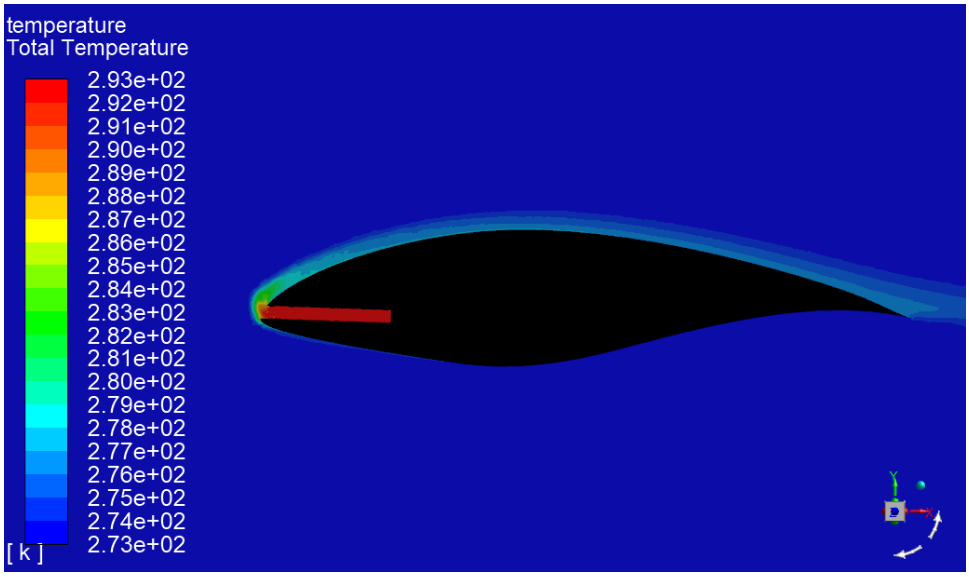

Figure 52. Temperature distribution at AoA=0º, β=+2º

3.4.Impact of Temperature and Pressure

In all the results given in the previous headings, the outdoor temperature, i.e. the temperature of the air in the tunnels, was taken as 0ºC. Hot air flowing through the pressure inlet is 20 ºC dry air with 3000 Pa pressure.

Finally, the effect of temperature and pressure on the lift with a small data set has been studied. For the case where the angle of attack is 0 degrees and the width is 2d,

simulations are made at different pressures and temperatures. The tables below give the operating conditions and the results for these comparisons.

Table 7. Pressure and temperature values

Design Point	β (degree)	Pressure Inlet Value (Pa)	Tunnel Temperature(K)
DP 17	-2	3000	273,15
DP 18	0	3000	273,15
DP 19	2	3000	273,15
DP 57	-2	2500	273,15
DP 58	0	2500	273,15
DP 59	2	2500	273,15
DP 60	-2	3000	263,15
DP 61	0	3000	263,15
DP 62	2	3000	263,15
DP 63	-2	2500	263,15
DP 64	0	2500	263,15
DP 65	2	2500	263,15

Table 8. Results of pressure and temperature variations

Design Point	c_l	Lower Surface Temperature(K)	Upper Surface Temperature(K)
DP 17	0,5962	278,60	273,15
DP 18	0,5802	277,35	274,30
DP 19	0,5577	277,12	274,36
DP 57	0,6015	278,34	273,15
DP 58	0,5929	275,99	273,80
DP 59	0,5834	274,03	275,11
DP 60	0,6225	270,85	263,15
DP 61	0,6098	268,96	264,81
DP 62	0,5897	264,72	268,28
DP 63	0,6267	270,54	263,15
DP 64	0,6253	266,70	263,99
DP 65	0,6144	264,24	265,60

As can be seen from the figure, an improvement in the lift was observed at a constant temperature when the pressure was reduced from 3000 Pa to 2500 Pa. The main reason for this is that 2500 Pa causes less deterioration in the pressure area around the wing. Thus, the loss of lifting is reduced while maintaining the hot film layer.

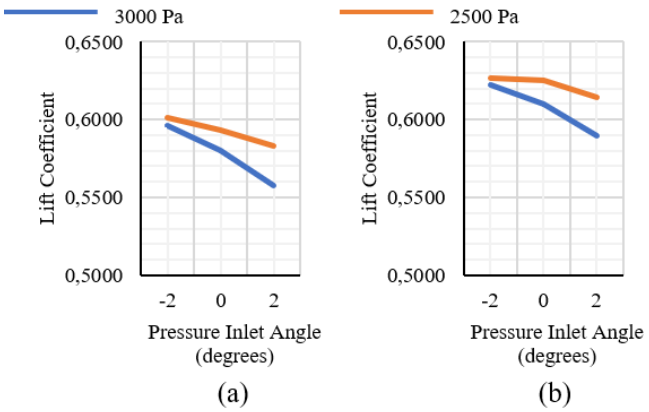

Figure 53. Comparison of different pressure values at constant temperatures

(a) Wind Temperature=273K, (b)Wind Temperature=263K

In addition, when Figure 53 (a) and (b) are compared, it can be seen that the lift changes depending on the temperature as well. Increased lift at cooler ambient temperature results from the increase in air density. This is basically a small proof of why wind turbines are installed in the cold first regions in the first place.

CHAPTER 4

CONCLUSION

With this study, a de/anti-ice design for the wind turbines is framed. By using the circular openings positioned on the wing profile, a thin film layer is formed on the wing and the effect of this layer on the aerodynamic performance is shown based on the design parameters.

Generally speaking, the simulation results of the selected S830 airfoil responded differently at positive attack angles and at the negative attack angles. At the negative attack angles, the relatively large diameter gap caused less loss in lifting performance.

In the lift curves drawn against the attack angle, it was observed that the lift moved more steadily as the width increased. The main reason for this is that as the w / d ratio increases, the effect of opening on the surface becomes insignificant. Because the pressure area that can be affected by the opening does not cause huge losses. But at this point, it is useful to see the contradiction. Less impact on the pressure field means less effect on the surface. And if the effect on the surface is reduced, the area covered by the hot film layer is becoming insufficient. In this case, the loss of a lift due to the opening, as well as ice cannot be prevented. For this reason, taking into account the lift performance, the surface temperatures should be taken into consideration when selecting the width.

As the distance between the openings has an effect on spreading the film through the span, the position of the opening at the tip region is also critical. Because the change in the pressure area along the wing profile is directly related to the flow of hot air from the opening towards the side of the wing. Considering the evaluation for the position of the opening, there is less loss of the lift if the hot air flows into the lower surface of the wing. However, the formation of the film layer only on the top or bottom surface is inefficient in terms of maintaining surface temperatures.

Another issue is the outlet pressure of the hot air released from the pressure inlet. The optimum state of this pressure can be observed when the hot fluid flows along the surface of the wing profile with minimal loss of performance. Results are presented in

which it is possible to improve aerodynamic performance by reducing the pressure of the hot fluid coming from the opening.

When the parameters of the current study are examined, the aerodynamic performance is better when the angle β is -2º, however, in the case of wrapping around the wing of the film layer, the cases where the angle β is 0º are achieved. This also opens a door to homogeneity in the temperature distribution on the wing surface.

REFERENCES

[1] D. A. Spera, *Wind Turbine Technology: Fundamental Concepts of Wind Turbine Engineering*, Second Edi. ASME, 2009.

[2] A. Sedaghat and M. Mirhosseini, "Aerodynamic design of a 300 kW horizontal axis wind turbine for province of Semnan," *Energy Convers. Manag.*, vol. 63, pp. 87–94, 2012.

[3] "VAWTs." [Online]. Available: https://www.treehugger.com/wind-technology/largest-vertical-axis-wind-turbine-installation-us-operating-texas-m.html%0A. [Accessed: 06-Apr-2019].

[4] L. Battisti, *Wind Turbines in Cold Climates: Icing Impacts and Mitigation Systems*. Springer, 2015.

[5] O. Parent and A. Ilinca, "Anti-icing and de-icing techniques for wind turbines: Critical review," *Cold Reg. Sci. Technol.*, vol. 65, no. 1, pp. 88–96, 2011.

[6] T. Wallenius and V. Lehtomäki, "Overview of cold climate wind energy: Challenges, solutions, and future needs," *Wiley Interdiscip. Rev. Energy Environ.*, 2016.

[7] M. C. Pedersen, H. Sørensen, N. Swytink-Binnema, B. Martinez, and T. Condra, "Measurements from a cold climate site in Canada: Boundary conditions and verification methods for CFD icing models for wind turbines," *Cold Reg. Sci. Technol.*, vol. 147, no. October 2017, pp. 11–21, 2018.

[8] N. Dalili, A. Edrisy, and R. Carriveau, "A review of surface engineering issues critical to wind turbine performance," *Renew. Sustain. Energy Rev.*, vol. 13, no. 2, pp. 428–438, 2009.

[9] T. Laakso, "Wind Energy Projects in Cold Climates," *Wind Energy*, pp. 1–36, 2005.

[10] C. Macarthur, J. Keller, and J. Luers, "Mathematical modeling of ice accretion on airfoils," 1982.

[11] C. Macarthur, "Numerical simulation of airfoil ice accretion," 1983.

[12] D. Guffond and L. Brunet, "Validation du programme bidimensionnel de capitation ONERA," 1988.

[13] R. W. Gent, "TRAJICE2 - A Combined Water Droplet Trajectory and Ice Accretion Prediction Program for Aerofoils," 1990.

[14] W. B. Wright, R. W. Gent, and D. Guffond, "DRA/NASA/ONERA Collaboration on Icing Research Part II-Prediction of Airfoil Ice Accretion," 1997.

[15] G. Fortin and J. Perron, “Wind turbine Icing and de-icing,” *47th AIAA Aerosp. Sci. Meet. Incl. New Horizons Forum Aerosp. Expo.*, 2009.

[16] L. Hu, X. Zhu, J. Chen, X. Shen, and Z. Du, “Numerical simulation of rime ice on NREL Phase VI blade,” *J. Wind Eng. Ind. Aerodyn.*, 2018.

[17] S. K. Thomas, R. P. Cassoni, and C. D. MacArthur, “Aircraft anti-icing and de-icing techniques and modeling,” *J. Aircr.*, vol. 33, no. 5, pp. 841–854, 1996.

[18] H. Seifert, “Technical Requirements for Rotor Blades Operating in Cold Climate,” *Proc. Boreas VI*, no. 24, pp. 50–55, 2003.

[19] I. Baring-Gould *et al.*, *Expert Group Study on Recommendations for wind energy projects in cold climates*. 2009.

[20] N. Technologies, “De-ice and anti-ice system and method for aircraft surfaces,” US 6194685 B1, 2001.

[21] Wobben Properties GmbH., “Rotor blade with heating device for a wind turbine,” US 20130309092 A1, 2013.

[22] G. A. L. Silva, O. M. Silvares, and E. J. G. J. Zerbini, “Numerical Simulation of Airfoil Thermal Anti-ice Operation, Part 1: Mathematical Modelling,” *J. Aircr.*, vol. 44, no. 2, pp. 627–633, 2007.

[23] O. A. Z. Rodríguez, “Numerical investigation of a wing hot air ice protection system,” no. December, p. 129, 2009.

[24] J. F. Maissan, “Wind Power Development In Sub-Arctic Conditions With Severe Rime Icıng,” in *Circumpolar Climate Change Summit and Exposition*, 2001.

[25] R. Karmouch, S. Coudé, G. Abel, and G. G. Ross, “Icephobic PTFE coatings for wind turbines operating in cold climate conditions,” in *2009 IEEE Electrical Power and Energy Conference, EPEC 2009*, 2009.

[26] A. D. Yaslik, K. J. De Witt, T. G. Keith, and W. Boronow, “Three-dimensional simulation of electrothermal deicing systems,” *J. Aircr.*, vol. 29, no. 6, pp. 1035–1042, 1992.

[27] J. John D. Anderson, *Fundamentals of Aerodynamics*, Fifth Edit. McGraw-Hill, 2011.

[28] ANSYS, “Ansys Fluent Theory Guide,” 2019.

[29] “Enercon Wind Turbine Spoiler.” [Online]. Available: https://www.evwind.es/2015/01/12/boralex-acquires-wind-farm-with-enercon-wind-turbines/49867. [Accessed: 22-Nov-2018].

[30] “Wind Turbine Tip.” [Online]. Available: https://ww-article-cache-1.s3.amazonaws.com/de/Enercon. [Accessed: 22-Nov-2018].